Design principles of transcription factors with intrinsically disordered regions

Wencheng Ji *[1,2], Ori Hachmo[1], Naama Barkai[3], and Ariel Amir †[1,2]

[1]Department of Physics of Complex Systems, Weizmann Institute of Science, 234 Hertzl St., Rehovot, Israel
[2]John A. Paulson School of Engineering and Applied Sciences, Harvard University, Cambridge, MA 02138, USA
[3]Department of Molecular Genetics, Weizmann Institute of Science, Rehovot, Israel

Abstract

Transcription Factors (TFs) are proteins crucial for regulating gene expression. Effective regulation requires the TFs to rapidly bind to their correct target, enabling the cell to respond efficiently to stimuli such as nutrient availability or the presence of toxins. However, the search process is hindered by slow diffusive movement and the presence of 'false' targets – DNA segments that are similar to the true target. In eukaryotic cells, most TFs contain an Intrinsically Disordered Region (IDR), which is commonly assumed to behave as a long, flexible polymeric tail composed of hundreds of amino acids. Recent experimental findings indicate that the IDR of certain TFs plays a pivotal role in the search process. However, the principles underlying the IDR's role remain unclear. Here, we reveal key design principles of the IDR related to TF binding affinity and search time. Our results demonstrate that the IDR significantly enhances both of these aspects. Furthermore, our model shows good agreement with experimental results, and we propose further experiments to validate the model's predictions.

Transcription Factors (TFs) are fundamental proteins that regulate gene expression: they bind to specific DNA sequences to control gene transcription [1]; they respond adaptively to various cellular signals, thereby modulating gene expression [2, 3]; they guide processes such as cell differentiation and development, and their malfunctions are often linked to disease onset [4, 5]. The principles of gene regulation were first formulated in the 1960s through pioneering studies of the *E. coli* Lac operon [6], establishing that the regulation mechanism is via the binding of a TF to the regulatory DNA regions associated with the genes, the TF's target. Effective regulation requires TFs to have sufficient binding affinity and a binding rate comparable to cellular processes. Despite these decades of research, the factors determining the binding strength and search efficiency of eukaryotic TFs remain incompletely understood [7, 8]. In eukaryotic cells, besides having a DNA-binding domain (DBD), approximately 80% of TFs also have one or more intrinsically disordered regions (IDRs), which lack a stable 3D structure and can be assumed as flexible, unstructured polymers, hundreds of amino acids (AAs) in length [9–12]. Eukaryotic DBDs often exhibit weaker affinity to their recognition sequences compared to their bacterial counterparts, indicating that IDRs are necessary for achieving stable binding [13]. However, IDRs are challenging to study because their functions can be maintained despite rapid sequence divergence, complicating traditional sequence-based analyses [14, 15]. Molecular dynamics simulations suggest that IDRs play a significant role in promoting target recognition [16], by

*wencheng.ji@weizmann.ac.il
†Corresponding author: ariel.amir@weizmann.ac.il

increasing the area of effective interaction between the TF and the DNA. Upon binding, the search problem becomes effectively a one-dimensional diffusion process [17]. Recent *in vivo* experiments done in yeast also suggest that IDRs could take a key part in guiding TFs to the DNA regions containing their targets [18, 19]. Truncation studies of IDRs in various TFs have demonstrated that removing these regions often results in reduced binding affinity, suggesting they contribute significantly to stabilizing TF-DNA interactions [18]. Different mechanisms have been proposed in the literature to explain IDR contributions: some suggest non-specific electrostatic interactions [20], others propose phase separation that concentrates TFs near their targets [21], while a third view suggests specific IDR-DNA interactions analogous to those of structured domains [22].

The problem of TF search has been widely studied, theoretically, albeit with the majority of works focusing on parameter regimes relevant for bacteria. One important mechanism is that of facilitated diffusion, in which the TF performs 1D diffusion along the DNA and at any given moment can fall off and perform 3D diffusion until reattaching to the DNA (a 3D excursion). The 1D diffusion along the DNA and the 3D excursions alternate until the TF finds its target. This mechanism is well characterized theoretically [23–29] and supported by experiments in *E. coli* [30]. However, due to the significant structural differences, including larger genome size and chromatin structure, the facilitated diffusion mechanism cannot explain the fast search times observed in eukaryotes, and a qualitatively different mechanism is required [7, 19, 31–33].

Here, we attempt to address the fundamental question of how IDRs can enhance the binding affinity of the TFs and speed up their search process, and to discover the associated design principles in eukaryotes. The problem of binding affinity (binding probability) exhibits the classical trade-off between energy and entropy: on one hand, the binding of IDR to the DNA is energetically favorable. On the other hand, this binding leads to constraints on the positions of the IDR (pinned to the DNA at the points of attachment) which leads to a reduction in the entropy associated with the possible polymer conformations – hence an *increase* in the free energy of the system. Therefore the effects of the disordered tail on affinity are non-trivial, leading to physical problems reminiscent of those associated with the well-studied problem of DNA unzipping [34]. We find that the binding probability increases dramatically for TFs having IDRs for a broad parameter regime. The optimal search process consists of one round of $3\mathrm{D}-1\mathrm{D}$ search, where at first the TF performs 3D diffusion and then binds the antenna and performs 1D diffusion until finding its target, rarely unbinding for another 3D excursion. This process is presented in Fig. 1**(a, c)**. We obtain an expression for the search time that shows good agreement with our numerical results.

Results

Binding probability of the TF from the equilibrium approach

The experiment described in Ref. [18] studied the binding affinity of wild-type and mutated TFs to their corresponding targets. They found that shortening the IDR length results in weaker affinity. To qualitatively model the binding affinity of a TF to its target, we utilize a well-known physical model of polymers, the Rouse Model [35, 36] (used in the subsequent dynamical section as well). See Materials and Methods. We note that our conclusions do not hinge on this choice, and our results hold also when using other polymer models (see Supplementary S1). Since the IDR is thought to recognize a relatively short flanking DNA sequence of the DBD target [18], we model a DNA segment as a straight-line "antenna" region [26, 37–39], where the IDR targets reside. We assume that the interaction between TF and DNA outside the antenna region is negligible. Note that the interaction between IDR and DNA is a specific interaction, with genomic localization determined by multivalent interactions mediated by hydrophobic residues [40, 41].

To gain an intuition into the binding probability of TF, we first study a TF with a single IDR site. From here on, energies will be measured in units of k_BT, to simplify our notation. We assume that the IDR has only one corresponding target. There are four possible states: neither the DBD nor the IDR are bound, the IDR is bound, the DBD is bound, and both are bound, which correspond to P_{free}, P_{IDR}, P_{DBD}, and P_{both}, respectively.

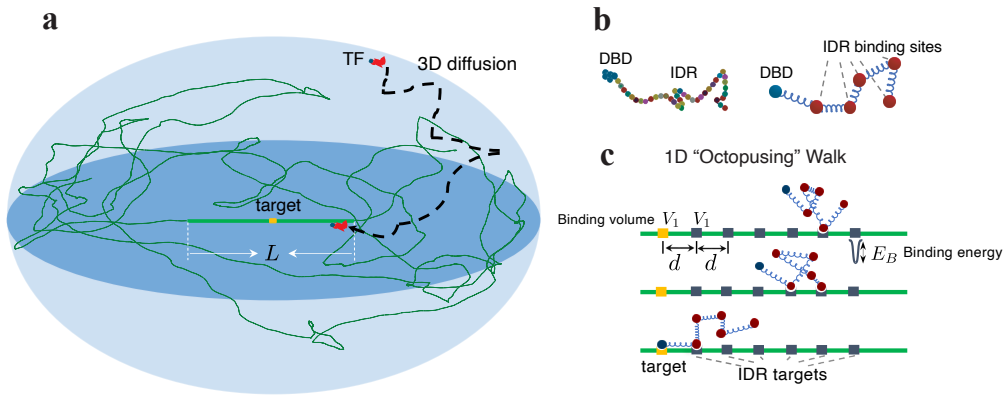

Figure 1: **Model illustration of a TF with the IDR and its search process.** **a**, Illustration of a TF locating its target site (highlighted in orange) on the DNA strand (depicted as a green curve). Surrounding the target is a region of length L, where the TF's IDR interacts with the DNA. The TF performs 3D diffusion until it encounters and binds to this "antenna" region. **b**, Illustration of a TF that includes an IDR composed of AAs. On the right: a model of the TF, a polymer chain, comprising of a single binding site on the DNA Binding Domain (DBD), and multiple binding sites on the IDR (also known as short linear motifs [8]). **c**, Once bound to the antenna, the TF performs effective 1D diffusion until it reaches its target. The 1D diffusion is via the binding and unbinding of sites along the IDR, a process we coin "octopusing". V_1 is the targets' volume, d the separation, and E_B the binding energy per binding site, where each site corresponds to a short linear motif.

The probability that the TF is bound at the DBD target is the sum of P_{DBD} and P_{both}. In thermal equilibrium, each of the 4 terms is given by the Boltzmann distribution, which can be solved analytically by integrating-out the additional degrees of freedom associated with the polymer (Supplementary S2). To better understand the associated design principles, it will be helpful to compare this probability with that of a "simple" TF (i.e., without the IDR), which we denote by P_{simple}. We find that:

$$\frac{P_{\text{TF}}}{P_{\text{simple}}} \approx (1+\mathcal{P}), \tag{1}$$

where $\mathcal{P}$ is an enhancement factor, governing the degree to which the IDR improved the binding affinity. Importantly, we find that:

$$\mathcal{P}(E_B, d, l_0) = e^{E_B} V_1 f(d, l_0), \tag{2}$$

where $f(d,l_0) = \left(\frac{3}{2\pi l_0^2}\right)^{3/2} \exp\left(-\frac{3d^2}{2l_0^2}\right)$, is the probability density, with units of inverse volume, V_1 is the targets' volume, on the order of $1-10\text{bp}^3$, as shown in Fig. 1**c**, $-E_B$ is the binding energy for per IDR target (E_B is always positive), d is the distance between the DBD target and the IDR target, and l_0 is the distance between the DBD and the IDR binding site on the TF (l_0 and d are also the distances for neighboring IDR targets and neighboring IDR sites, respectively, in the case of multiple IDR targets and sites). This shows that the presence of the IDR always increases the binding affinity since $\mathcal{P}$ is always positive. However, the magnitude of enhancement can be negligible: For instance, even if E_B is large, the term $f(d,l_0)$, associated with the entropic penalty (because the end-to-end distance is fixed, reducing the degrees of freedom compared to a free polymer), could lead to small values of $\mathcal{P}$. The exponential decay of $\mathcal{P}$ with d^2 (through the term $f(d,l_0)$), indicates that placing the IDR targets close to the DBD target is preferable. However, due to physical limitations, d cannot be arbitrarily small and in reality will have a lower bound. Once d is fixed, $\mathcal{P}$ is maximal at $l_0 = d$, as can be gleaned from equation (2). This condition minimizes the free energy penalty associated with the entropic contribution of the term $f(d,l_0)$. As we shall see, this design principle is also intact when multiple IDR sites and targets are involved, which is the scenario

we discuss next.

A *priori*, it is unclear whether having more binding sites ($n_b > 1$) on the IDR or more targets ($n_t > 1$) on the DNA will be beneficial or not. We therefore sought to investigate how the binding affinity depends on these parameters, as well as the binding energy and positions of the targets and binding sites. This generalization requires taking into account all the possible number of bindings, n (ranging from 0 to $\min(n_b, n_t)$), and all possibilities for binding orientations for each n, $\binom{n_b}{n}\binom{n_t}{n}n!$ distinct configurations in total. For each of them, we may analytically integrate-out the polymer degrees of freedom and calculate explicitly the contribution to the partition function (Supplementary S2). Summing these terms together, numerically, allows us to explore how the different parameters affect the binding specificity, which we describe next. To characterize the binding affinity, we resort again to the ratio $Q \equiv P_{\mathrm{TF}}/P_{\mathrm{simple}}$, measuring the effectiveness of the binding in comparison to the case with no IDRs. The length of TFs in our considerations, which varies with n_b, is comparable to that in experiments [18].

We find the design principle: $l_0 = d$, identical to what we showed for the case of a single IDR binding site. Specifically, Q is maximal at $l_0 \sim d$ for all combinations of n_b and n_t. Fig. 2**a** displays this principle for several combinations of n_b and n_t. All combinations are provided in Supplementary Fig. S3. This is plausible since for the IDR to be bound to the DNA at multiple places without paying a large entropic penalty, the distance between target sites should be compatible with the distance between binding sites. We therefore set $l_0 = d$ and search for other design principles. Fig. 2**b** shows a heatmap of Q varying with n_b and n_t. At large n_t, as n_b increases, the value of P_{TF} exhibits an initial substantial increase, followed by a gradual rise until it reaches saturation (shown explicitly in Supplementary Fig. S4). A similar behavior is also observed when varying the value of n_t. (When n_t exceeds n_b, the contribution from the states where the IDR is bound but the DBD is unbound increases with increasing n_t, which slightly lowers P_{TF}; see Supplementary Fig. S4.) In fact, the heatmap shown in Fig. 2**b** shows that the value of P_{TF} is governed, approximately, by the *minimum* of n_b and n_t (this is reflected in the nearly symmetrical "L-shapes" of the contours). This places strong constraints on the optimization, and suggests that there will be little advantage in increasing the value of either n_b or n_t beyond the point $n_b = n_t$, revealing another design principle (under the assumption that it is preferable to have smaller values of n_b and n_t for a given level of affinity, in order to minimize the cellular costs involved). We verify this principle holds at additional values of E_B. Fig. 2**c** shows that the contours corresponding to $P_{\mathrm{TF}} = 0.9$ at varying values of E_B all take an approximate symmetrical L-shape, thus supporting the design principle $n_b = n_t$. For a given E_B, we denote the optimal values as $n_b^* = n_t^*$, and show them as hexagrams in the plot. We further find that n_b^* decreases with increasing E_B, as displayed in the inset. These relationships also hold at $P_{\mathrm{TF}} = 0.5$ (Supplementary S5).

We examine the variation of Q with respect to E_B while keeping $n_b = n_t$ constant. In Fig. 2**d**, as the binding energy E_B increases, Q increases from a value of ~ 1 to its saturation value, $1/P_{\mathrm{simple}}$, in a switch-like manner: i.e., there is a characteristic energy scale, E_{th}. To estimate E_{th}, when $Q \ll 1/P_{\mathrm{simple}}$ (i.e., $P_{\mathrm{TF}} \ll 1$), we approximate the expression of Q as:

$$Q \approx 1 + \Sigma_{n=1}^{n_b} \Sigma_{\mathrm{orn}} \prod_{i=1}^{n} \mathcal{P}(E_B, r_{\mathrm{orn},i}, l_{\mathrm{orn},i}), \tag{3}$$

where $l_{\mathrm{orn},i}$ and $r_{\mathrm{orn},i}$ denote the segment length between two adjacent bound sites and the distance associated with their respective targets, respectively, and "orn" represents the orientation of the given configuration (Supplementary S2). Equation (3) reduces to equation (1) when $n_t = n_b = 1$. To substantially increase Q, the configuration that contributes the most to Q, would satisfy $(\mathcal{P}(E_B, d, d))^{n_b} \gg 1$. Thus, the characteristic energy E_{th} could be estimated using the formula $\mathcal{P}(E_{\mathrm{th}}, d, d) = 1$, resulting in:

$$E_{\mathrm{th}} = \frac{3}{2}\left[\ln\left(\frac{2\pi}{3\phi^2}\right) + 1\right], \tag{4}$$

where $\phi = V_1^{1/3}/d$ represents the proportion of IDR targets within the antenna. Equation (4) is a direct consequence

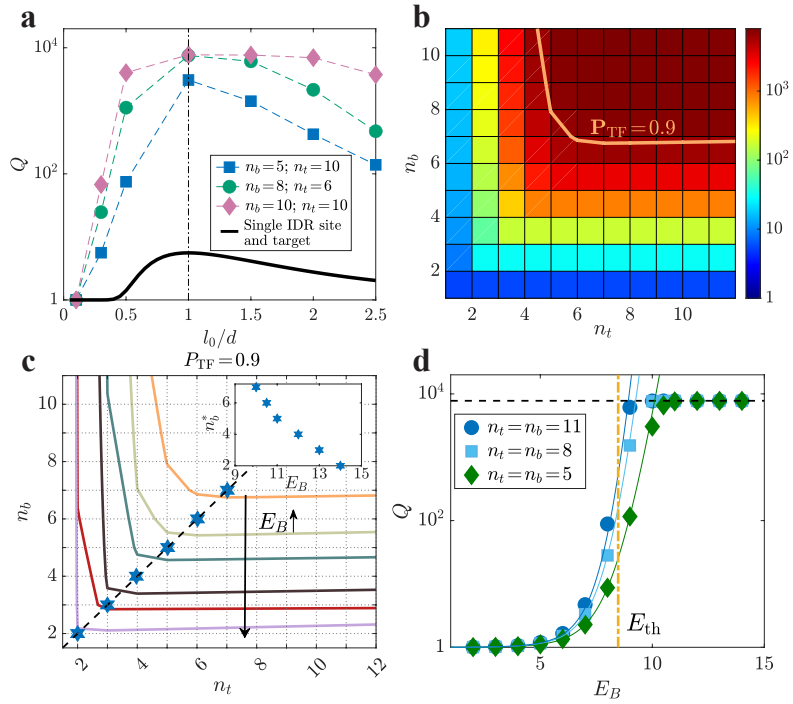

Figure 2: **Design principles across various parameters:** l_0/d**,** n_b**,** n_t**, and** E_B**.** **a**, Plots of $Q \equiv P_{\rm TF}/P_{\rm simple}$ varying with l_0/d are shown for several combinations of n_t and n_b for typical values of the relevant quantities: the nucleus volume is $1\mu{\rm m}^3$, $E_{\rm DBD}=15$, $E_B=10$, $V_1=(0.34{\rm nm})^3$, and $d=\sqrt{50}\cdot 0.34{\rm nm}$. **b**, A heatmap of Q vs. n_b and n_t at $E_B=10$ and $d=l_0$. **c**, Contour lines at different E_B at $P_{\rm TF}=0.9$. Blue hexagrams represent the design principle $n_b^*=n_t^*$, with the black dashed line as a visual guide. The inset shows the dependence of n_b^* on energy. **d**, Q for varying E_B at $d=l_0$ for several $n_b=n_t$. The vertical line represents $E_{\rm th}$ as determined by equation (4), the solid curves illustrate the approximation of Q obtained from equation (3), and the horizontal line indicates where $P_{\rm TF}=1$.

of the energy-entropy trade-off. Increasing ϕ leads to a decrease in entropy loss due to binding the IDR, subsequently reducing the demands on binding energy. Given that $\phi^2=0.02$, $E_{\rm th}$ is about $8.5k_BT$. The vertical dashed line in Fig. 2**d**, obtained from equation (4), effectively captures the region of significant increase for large values of n_b. Hence, we obtain the third design principle: $E_B > E_{\rm th}$, which ensures the significant binding advantage of TFs with IDRs.

So far, we have found that the binding design principles for TFs with IDRs are as follows: (**i**) target distance d should be as small as possible, (**ii**) IDR segment binding distance l_0 should be comparable to d, (**iii**) it is preferable to have fewer binding sites n_b^* and binding targets n_t^* as the binding strength E_B increases, with $n_b^*\sim n_t^*$, and (**iv**) E_B should be larger than a threshold that solely depends on the proportion ϕ of IDR targets within the antenna, as indicated by Eq. (4). In our estimation, with $\phi^2=0.02$, we obtain $E_{\rm th}\approx 8.5k_BT$. The above principles have also been validated in scenarios involving Poisson statistics of binding site distances and target distances, thus indicating their robust applicability (Supplementary Fig. S6).

Search time of the TF from the dynamics

In this section, we study the design principles of the TF *search time*, a dynamic process. Here, we confine the TF with $\tilde{n}\equiv n_b+1$ sites (n_b IDR sites and one DBD site) to a sphere of radius R, the cell nucleus, and use over-damped

coarse-grained molecular dynamics (MD) simulations. The sites and targets interact via a short-range interaction. The DBD target with a radius a is placed at the sphere's center. See the sketch in Fig. 1**a**. Once the DBD finds its target, the search ends. We denote the mean total search time (i.e., the mean first passage time, MFPT), as $t_{\rm total}$. We estimate it by averaging 500 simulations, each starting from an equilibrium configuration of the TF at a random position in the nucleus. Simulation details are provided in the Materials and Methods section.

By conducting comprehensive simulations of $t_{\rm total}$ across various parameter values of L, E_B, and $\tilde{n}$, we were able to identify its minimum value, which is approximately at $L^* = 300{\rm bp}$, $E_B^* = 11$, and $\tilde{n}^* = 4$ for $R = 500{\rm bp} \approx 1/6\mu{\rm m}$. Here, one base pair (bp) is equal to $0.34{\rm nm}$. To speed up the simulations, we utilized several computational tricks, including adaptive time steps and treating the TF as a point particle when it is far from the antenna (see Materials and Methods). Despite of this, the simulations require 10^5 CPU hours due to the IDR trapped in the binding targets on the antenna, which results in the slow dynamics as found in the previous simulation works [16, 42]. The probability distribution function (pdf) of individual search times exponentially decays with a typical time equal to $t_{\rm total}$, see inset of Fig. 3. This indicates that $t_{\rm total}$ provides a good characterization of the search time.

We find that $t_{\rm total}$ varies non-monotonically with L at fixed E_B^* and $\tilde{n}^*$ as shown in Fig. 3. Once a TF attaches to one of its targets, it will most likely diffuse along the antenna until reaching the DBD target (Supplementary S7). It means that the optimal search process is a single round of 3D diffusion followed by 1D diffusion along the antenna. In Supplementary S8, by analytically calculating the mean total search time using a coarse-grained model, we find that a single round of 3D-1D search is typically the case in the optimal search process. Note that our model differs profoundly from the conventional facilitated diffusion (FD) model in bacteria: In the latter, the TF is assumed to bind non-specifically to the DNA. Within our model, the antenna length L can be tuned by changing the placement of the IDR targets on the DNA, making it an adjustable parameter rather than the entire genome length. As opposed to the FD model, which requires numerous rounds of DNA binding-unbinding to achieve minimal search time, within our model, the minimal search time is achieved for a single round of 3D and 1D search.

Interestingly, when we observe the motion of a TF along the antenna, IDR sites behave like "tentacles", as illustrated in Fig. 1**c**, constantly binding and unbinding from the DNA. We refer to this 1D walk as "octopusing", inspired by the famous "reptation" motion in entangled polymers suggested by de Gennes [43] (see Supplementary Video). We note that previous numerical studies [16, 17] used comprehensive, coarse-grained, MD simulations to demonstrate that including heterogeneously distributed binding sites on the IDR could facilitate intersegmental transfer between different regions of the DNA, which is reminiscent of our octopusing scenario.

The mean 3D search time, $t_{\rm 3D}$, and the mean 1D search time, $t_{\rm 1D}$ are also shown in Fig. 3. To evaluate $t_{\rm 3D}$, we take advantage of several insights: first, if the TF gyration radius, $r_p = \sqrt{\tilde{n}/6}l_0$, is comparable or larger than the distance between targets, d, we may consider the chain of targets as, effectively, a continuous antenna. Making the targets denser would hardly accelerate the search time, reminiscent of the well-known chemoreception problem where high efficiency is achieved even with low receptor coverage [44]. Second, when the distance between the TF and the antenna is smaller than r_p, one of the binding sites on the TF would almost surely attach to the targets. This allows us to approximately map the problem to the MFPT of a particle hitting an extremely thin ellipsoid with long-axis of length L and radius r_p, the solution of which is $\ln(L/r_p)/L$ [45]. We find that this scaling captures well the dependence of $t_{\rm 3D}$ on the parameters, with a prefactor $\alpha \sim O(1)$. For the 1D search from a single particle picture, since the TF is unlikely to detach once it attaches, it performs a 1D random walk. So, taken together, the mean total search time is

$$t_{\rm total} = t_{\rm 3D} + t_{\rm 1D} \approx \alpha \frac{\tilde{n}R^3}{DL} \ln(L/r_p) + \beta \frac{L^2}{D}, \tag{5}$$

where D is the 3D diffusion coefficient of one site. For a TF with $\tilde{n}$ sites, its 3D diffusion coefficient, D_3, is $D/\tilde{n}$. α and β are fitting parameters. The semi-analytical formulas of $t_{\rm 1D}$, $t_{\rm 3D}$, and $t_{\rm total}$, denoted by the solid lines in Fig. 3, agree well with the simulation results for $\alpha = 0.5$ and $\beta = 14.5$. The theoretical result for the time spent in 3D was originally calculated for a point searcher [45]. In that case, a value of $\alpha = 2/3$ was obtained. β is larger at

larger E_B (see Supplementary S7).

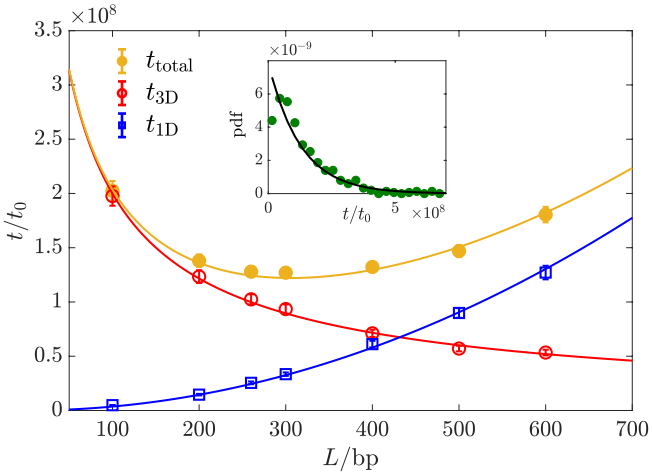

Figure 3: **Mean search time varying with the antenna length** L. t_{total}, $t_{3\text{D}}$ and $t_{1\text{D}}$ vs. L at E_B^* and $\tilde{n}^*$. The solid curves correspond to t_{total} , $t_{3\text{D}}$ and $t_{1\text{D}}$ in equation (5). Inset: probability density function (pdf) exponentially decays at large t. pdf $\approx \exp(-t/t_{\text{total}})/t_{\text{total}}$ (black solid line). The unit t_0 represents the time for one AA to diffuse 1bp. $a = 0.5$bp, $d = 10$bp, and $l_0 = 5$bp.

We also examine the dependence of t_{total} on the key parameters E_B and $\tilde{n}$, in the vicinity of the optimal parameters which minimize the total search time (Supplementary S7). We find that the affinity of TFs to the antenna decreases rapidly with decreasing the IDR length [18] and E_B. Consequently, when $\tilde{n} < \tilde{n}^*$ or $E_B < E_B^*$, multiple search rounds are needed to reach the DBD target, resulting in a significant escalation of t_{total}. When $\tilde{n} > \tilde{n}^*$, t_{total}, $t_{3\text{D}}$, and $t_{1\text{D}}$ agree with equation (5). When $E_B > E_B^*$, since $t_{3\text{D}}$ is independent of E_B, the variation in t_{total} stems from $t_{1\text{D}}$ which exponentially increases with E_B.

The minimal search time for a simple TF is $t_{\text{simple}} = R^3/(3Da)$ [45]. For the TF with an IDR, by minimizing the expression in equation (5), we find that the optimal length approximately scales as $L^* \propto R$, and therefore the minimal search time, t_{min}, is approximately proportional to R^2. At $R = 500\,\text{bp} \approx 1/6\mu\text{m}$, the search time is more than ten times shorter than a simple TF, despite the latter's diffusion coefficient being several times larger. Based on our analytic result, we expect ~ 50 fold enhancement for the experimental parameters of yeast (note that we assume the scaling $t_{\text{min}} \sim R^2$ still holds in this regime; this formula is approximate since it does not take into account the persistence length of DNA [46], which is several-fold shorter than the optimal antenna length L^*. We have verified that reducing the DNA persistence length, which promotes increased DNA coiling, results in only a modest increase in mean search time. Even under extreme coiling conditions, the increase remains below 30% of the baseline value, as detailed in Supplementary S9. Converting t_{min} into a second-order on-rate yields approximately $10^8 - 10^9\,\text{M}^{-1}s^{-1}$, assuming $D \approx 10^{-13}m^2/s$ and a TF copy number of 100. We also verified that the 3D diffusion coefficient slightly changes under a complex DNA configuration, where a point-searcher TF non-specifically interacts with the entire DNA, indicating the robustness of our optimal search process (see Supplementary S10).

Next, we characterize the dynamics of the octopusing walk (Supplementary S11). During this process, different IDR binding sites constantly bind and unbind from the antenna, leading to an effective 1D diffusion. A *priori*, one may think that the TF faces conflicting demands: it has to rapidly diffuse along the DNA while also maintaining strong enough binding to prevent detaching from the DNA too soon. Indeed, within the context of TF search in bacteria, this is known as the speed-stability paradox [25]. Importantly, the simple picture of the octopusing walk explains an elegant mechanism to bypass this paradox, achieving a high diffusion coefficient with a low rate of detaching from the DNA. This comes about due to the compensatory nature of the dynamics: there is, in effect, a

feedback mechanism whereby if only a few sites are bound to the DNA, the on-rate increases, and similarly, if too many are bound (thus prohibiting the 1D diffusion) the off-rate increases. Remarkably, this mechanism remains highly effective even when the typical number of binding sites is as low as two. Further details are provided in Supplementary S11.

Comparing with experimental results

In Ref. [18], the binding probability of the TF Msn2 in yeast was measured, where the native IDR was shortened by truncating an increasingly large portion of it. The results indicate that binding probability decreases with increasing truncation of the IDR, as illustrated in Fig. 4(a). We utilized our model to calculate the relative binding probability compared to P_{TF} at a zero truncating length. Using the DBD binding energy E_{DBD} as our only fitting parameter, our model achieves quantitative agreement with the experimental data. In Fig. 4(b), we estimate the search time as a function of L for $R = 1\mu m$ and $D_0 = 10^{-10} m^2/s$ for a single AA. The estimated timescales are comparable to empirical results, which are 1 to 10 seconds [19, 47], as indicated by the shaded area. We have also estimated the on-rate k_{on} and off-rate k_{off} of the TF as they vary with IDR length, as shown in Fig. 4(c). In the kinetic proofreading mechanism [48], specificity is associated with the off-rate, but recent studies [49] suggest that in other scenarios, specificity is encoded in the on-rate. Therefore, it is important to explore how specificity is encoded within this mechanism. Our results indicate that the variation in the dissociation constant $k_{\mathrm{off}}/k_{\mathrm{on}}$ is dominated by k_{off}, suggesting that specificity is encoded in the off-rate. The magnitudes and variations of these rates could be directly compared to experimental results in future studies.

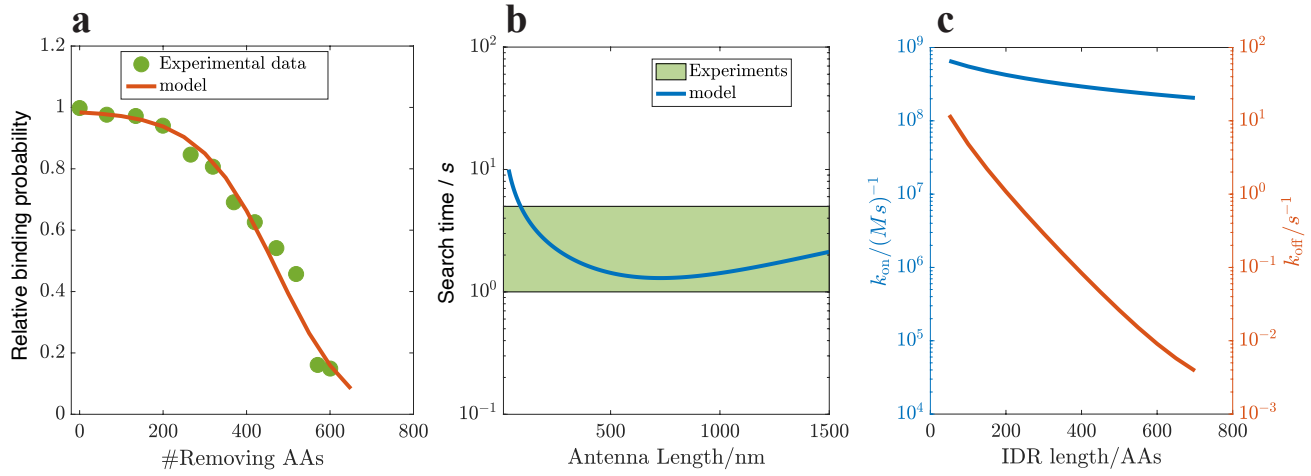

Figure 4: **a**, Relative binding probability varies with the truncation length of the IDR, which quantitatively agrees with the experimental data in Ref. [18], where we only vary E_{DBD} (binding energy of DBD) to ensure that the maximal value reaches 1 at zero truncation length. Antenna length $L = 1000\mathrm{nm}$, $E_{\mathrm{DBD}} = 22$ and $E_B = 11$. Other parameters are set the same as in Fig. 2. **b**, The search time estimated by our model (from Eq. (5) and divided by a TF copy number of 100) is quantitatively comparable with the experimental results [47], as guided by the shaded area. **c**, The on-rate $k_{\mathrm{on}} = t_{\mathrm{total}}/V_c$ and off-rate $k_{\mathrm{off}} = (1 - P_{\mathrm{TF}})/(P_{\mathrm{TF}} t_{\mathrm{total}})$ varying with the IDR length, indicating that $k_D \equiv k_{\mathrm{off}}/k_{\mathrm{on}}$ ranges from 0.01 to 10 nM, with its variation primarily dominated by the off-rate.

Conclusion and Discussion

In summary, we addressed the design principles of TFs containing IDRs, with respect to binding affinity and search time. We find that both characteristics are significantly enhanced compared to simple TFs lacking IDRs.

The simplified model we presented provides general design principles for the search process and testable predictions. One possible experiment that could shed light on one of our key assumptions is "scrambling" the DNA (randomizing the order of nucleotides). Our results depend greatly on our assumption that there exists a region on the DNA, close to the DBD target, that contains targets for the IDR binding sites. It is possible to shuffle, or even remove, regions of different lengths around the DBD target and to measure the resulting changes in binding affinity. According to our results, we would expect that shuffling a region smaller in length than the IDR should have minimal effect on the binding affinity and search time, but that shuffling a region longer than the IDR should have a noticeable effect.

Another useful test of our model would be to probe the *dynamics* of the TF search process by varying the waiting time before TF-DNA interactions are measured: Within the ChEC-seq technique [50] employed in Ref. [18], an enzyme capable of cutting the DNA is attached to the TF, and activated at will (using an external calcium signal). Sequencing then informs us of the places on the DNA at which the TF was bound at the point of activation. Measuring the binding probabilities at various waiting times — defined as the time between adding calcium ions and adding transcription factors, ranging from seconds to an hour, would inform us both of the TF search dynamics as well as the equilibrium properties: Shorter time scales would capture the dynamics of the search process, while longer time scales would reveal the equilibrium properties of the binding. At short waiting times (within several seconds), we would expect the binding probability to increase with waiting times. By analyzing a normalized binding probability curve as a function of the waiting time t, we could fit the curve using the function $1-\exp(-t/t_{\text{search}})$. From this curve, we can infer the search time. Our results suggest that the presence of the IDR in a TF leads to increased binding probabilities over various waiting times and a reduced waiting time to reach a higher saturation binding probability. Furthermore, as shown in Fig. 4 obtained from our model, k_{on} can be determined from the measurements of t_{search}. Using the binding probability, which is associated with $k_D = k_{\text{off}}/k_{\text{on}}$, k_{off} can also be calculated.

While our work primarily focused on coarse-grained modeling of the search process and the hypothesized octopusing dynamics, higher-resolution molecular dynamics simulations could provide more detailed molecular insights and further validate our proposed design principles [16, 17]. Since these principles are grounded in fundamental physical concepts, such as the energy-entropy trade-off, they are likely to be robust across diverse molecular systems. We anticipate their applicability to other biophysical contexts, such as nonspecific RNA polymerase binding [51] and multivalent antibody binding [52], where the associated dynamic processes would also be of significant interest for future research. Beyond our octopusing mechanism, other mechanisms may also contribute to the search and binding process. IDRs could facilitate complex formation and cooperativity between multiple transcription factors, as suggested by studies showing co-localization at common target promoters [53]. IDRs might also enhance efficiency by directing transcription factors to specific nuclear compartments or biomolecular condensates, thereby reducing the effective search space and time [21, 54, 55]. These complementary mechanisms [7, 8, 56] suggest that our findings represent one component of a broader regulatory framework governing transcriptional control in eukaryotic cells.

Acknowledgements: We thank Samuel Safran, David Mukamel, Yariv Kafri, Yaakov Levy, Luyi Qiu, and Zily Burstein for insightful discussions. We thank the Clore Center for Biological Physics for their generous support.

Materials and Methods

Model: The Rouse Model describes a polymer as a chain of point masses connected by springs and characterized by a statistical segment length l_0 resulting from the rigidity of springs k and the thermal noise level k_BT, $l_0^2 = 3k_BT/k$ [35, 36]. We coarse-grain the TF by representing it with a few binding sites for the IDR, and an additional site for the DBD, as illustrated in Fig. 1**b**. The targets are assumed to be positioned at equal spacing, with one target for the DBD and a few targets for the IDR, corresponding to the orange and black squares in Fig. 1**c**. We have also verified that relaxing this assumption, and using randomly positioned targets, does not affect our results (Supplementary S6). In the Rouse Model, the 3D probability density describing the relative distance in the equilibrium state, denoted as r, between any two sites can be derived through Gaussian integration [36], leading to:

$$f(r,l) = \left(\frac{3}{2\pi l^2}\right)^{\frac{3}{2}} \exp\left(-\frac{3r^2}{2l^2}\right), \tag{6}$$

where $l = \sqrt{n_{\text{seg}}}l_0$ and n_{seg} is the number of segments between the two sites.

Dynamical simulations: Each binding site of the TF at position $\boldsymbol{r}_i$ follows over-damped dynamics, which reads:

$$\Delta\boldsymbol{r}_i = \frac{D}{k_BT}\boldsymbol{f}(\{\boldsymbol{r}_i\})\Delta t + \sqrt{2D\Delta t}\,\boldsymbol{\xi}, \tag{7}$$

where the random variable ξ follows the standard normal distribution. D is the diffusion coefficient of the coarse-grained binding site. The force acting on each site is $\boldsymbol{f}(\{\boldsymbol{r}_i\}) \equiv -\partial U_{\text{total}}/\partial\boldsymbol{r}_i$, and

$$U_{\text{total}} = \sum_{i=0}^{n_b-1}\frac{1}{2}k(\boldsymbol{r}_{i+1}-\boldsymbol{r}_i)^2 + \sum_{i,j}E_B\exp\left[-\frac{(\boldsymbol{r}_i-\boldsymbol{R}_j)^2}{2w_d^2}\right], \tag{8}$$

where $\boldsymbol{R}_j$ are the positions of the targets. $w_d = 1\text{bp}$ is the typical width of the short-range interaction between sites and their corresponding targets. The typical distance l_0 between coarse-grained binding sites is 5bp. The stiffness of the springs is thus $3k_BT/l_0^2 = 3k_BT/25\text{bp}^2$. To speed up the simulations, when the sites' minimal distance to the antenna is larger than the threshold 10bp, the TF is regarded as a rigid body, and all sites move in sync with their center of mass. We verified that the resulting search time is insensitive to the value of this threshold. When the sites' minimal distance to the antenna is less than 10bp, we consider the excluded volume effect to ensure that different binding sites are not trapped at the same target. Specifically, we use the WCA interaction [57]:

$$U_{\text{WCA}} = \begin{cases} \frac{\sigma^{12}}{|\boldsymbol{r}_i-\boldsymbol{r}_j|^{12}} - \frac{2\sigma^6}{|\boldsymbol{r}_i-\boldsymbol{r}_j|^6} + 1, & |\boldsymbol{r}_i-\boldsymbol{r}_j| < \sigma \\ 0, & |\boldsymbol{r}_i-\boldsymbol{r}_j| \geq \sigma \end{cases} \tag{9}$$

where $\sigma = 1\text{bp}$. In this region, we also adopted an adaptive time step: $\Delta t/(\text{bp}^2/D) = \min\left\{1, \frac{k_BT}{\max|\boldsymbol{f}_i|\,\text{bp}}\right\}\times 0.01$. Note that this choice ensures that the displacement of the sites at every step is much smaller than the binding site size w_d. Due to the IDR trapped in the binding targets on the antenna, which results in slow dynamics, the simulation time becomes significantly longer, as found in previous simulation studies [16, 42]. This slowdown is similar to the behavior observed in glass-forming liquids [58]. As a result, the individual simulation time steps range from 10^9 to 10^{11}.

Declarations

- The authors declare no competing interests.
- Data and code availability: The data supporting this study's findings and the codes used in this study are available from W. Ji and the corresponding author.
- Authors' contributions: All authors contributed to the design of the work, analysis of the results, and the writing of the paper.

References

[1] David S. Latchman. Transcription factors: An overview. The International Journal of Biochemistry; Cell Biology, 29(12):1305–1312, December 1997. ISSN 1357-2725. doi: 10.1016/s1357-2725(97)00085-x. URL http://dx.doi.org/10.1016/S1357-2725(97)00085-X.

[2] Pamela J. Mitchell and Robert Tjian. Transcriptional regulation in mammalian cells by sequence-specific dna binding proteins. Science, 245(4916):371–378, July 1989. ISSN 1095-9203. doi: 10.1126/science.2667136. URL http://dx.doi.org/10.1126/science.2667136.

[3] Mark Ptashne and Alexander Gann. Transcriptional activation by recruitment. Nature, 386(6625):569–577, April 1997. ISSN 1476-4687. doi: 10.1038/386569a0. URL http://dx.doi.org/10.1038/386569a0.

[4] Samuel A. Lambert, Arttu Jolma, Laura F. Campitelli, Pratyush K. Das, Yimeng Yin, Mihai Albu, Xiaoting Chen, Jussi Taipale, Timothy R. Hughes, and Matthew T. Weirauch. The human transcription factors. Cell, 172(4):650–665, February 2018. ISSN 0092-8674. doi: 10.1016/j.cell.2018.01.029. URL http://dx.doi.org/10.1016/j.cell.2018.01.029.

[5] Ralph Stadhouders, Guillaume J. Filion, and Thomas Graf. Transcription factors and 3d genome conformation in cell-fate decisions. Nature, 569(7756):345–354, May 2019. ISSN 1476-4687. doi: 10.1038/s41586-019-1182-7. URL http://dx.doi.org/10.1038/s41586-019-1182-7.

[6] François Jacob and Jacques Monod. Genetic regulatory mechanisms in the synthesis of proteins. Journal of Molecular Biology, 3:318–356, June 1961. doi: 10.1016/s0022-2836(61)80072-7. URL https://doi.org/10.1016/s0022-2836(61)80072-7.

[7] John J Ferrie, Jonathan P Karr, Robert Tjian, and Xavier Darzacq. "structure"-function relationships in eukaryotic transcription factors: The role of intrinsically disordered regions in gene regulation. Molecular Cell, 2022. URL https://doi.org/10.1016/j.molcel.2022.09.021.

[8] Felix Jonas, Yoav Navon, and Naama Barkai. Intrinsically disordered regions as facilitators of the transcription factor target search. Nature Reviews Genetics, 26:424–435, February 2025. doi: 10.1038/s41576-025-00816-3. URL https://doi.org/10.1038/s41576-025-00816-3.

[9] Jiangang Liu, Narayanan B. Perumal, Christopher J. Oldfield, Eric W. Su, Vladimir N. Uversky, and A. Keith Dunker. Intrinsic disorder in transcription factors. Biochemistry, 45(22):6873–6888, May 2006. URL https://doi.org/10.1021/bi0602718.

[10] Monika Fuxreiter, Istvan Simon, and Sarah Bondos. Dynamic protein–DNA recognition: beyond what can be seen. Trends in Biochemical Sciences, 36(8):415–423, August 2011. doi: 10.1016/j.tibs.2011.04.006. URL https://doi.org/10.1016/j.tibs.2011.04.006.

[11] Xin Guo, Martha L Bulyk, and Alexander J Hartemink. Intrinsic disorder within and flanking the dna-binding domains of human transcription factors. In Biocomputing 2012, pages 104–115. World Scientific, 2012. URL https://doi.org/10.1142/9789814366496_0011.

[12] Peter E. Wright and H. Jane Dyson. Intrinsically disordered proteins in cellular signalling and regulation. Nature Reviews Molecular Cell Biology, 16(1):18–29, December 2014. doi: 10.1038/nrm3920. URL https://doi.org/10.1038/nrm3920.

[13] Daniel A. Garcia, Wei-Ting Chen, Shuying Ren, Long-Chi Chen, Xiaonan Chen, Shiqi Yu, Zhijie Han, Sergei Kalugin, Ken Kono, Roberta Noberini, et al. An intrinsically disordered region-mediated confinement state contributes to the dynamics and function of transcription factors. Molecular Cell, 81(7):1484–1498, 2021. doi: 10.1016/j.molcel.2021.01.013. URL https://doi.org/10.1016/j.molcel.2021.01.013.

[14] Celeste J. Brown, Audra K. Johnson, and Gary W. Daughdrill. Comparing models of evolution for ordered and disordered proteins. Molecular Biology and Evolution, 27(3):609–621, March 2010. doi: 10.1093/molbev/msp277. URL https://doi.org/10.1093/molbev/msp277.

[15] Taraneh Zarin, Bob Strome, Alex N Nguyen Ba, Simon Alberti, Julie D Forman-Kay, and Alan M Moses. Proteome-wide signatures of function in highly diverged intrinsically disordered regions. eLife, 8:e46883, jul 2019. ISSN 2050-084X. doi: 10.7554/eLife.46883. URL https://doi.org/10.7554/eLife.46883.

[16] Dana Vuzman and Yaakov Levy. Dna search efficiency is modulated by charge composition and distribution in the intrinsically disordered tail. Proceedings of the National Academy of Sciences, 107(49):21004–21009, 2010. URL https://doi.org/10.1073/pnas.1011775107.

[17] Dana Vuzman and Yaakov Levy. Intrinsically disordered regions as affinity tuners in protein–dna interactions. Molecular Biosystems, 8(1):47–57, 2012. URL https://doi.org/10.1039/c1mb05273j.

[18] Sagie Brodsky, Tamar Jana, Karin Mittelman, Michal Chapal, Divya Krishna Kumar, Miri Carmi, and Naama Barkai. Intrinsically disordered regions direct transcription factor in vivo binding specificity. Molecular Cell, 79(3):459–471.e4, August 2020. URL https://doi.org/10.1016/j.molcel.2020.05.032.

[19] Divya Krishna Kumar, Felix Jonas, Tamar Jana, Sagie Brodsky, Miri Carmi, and Naama Barkai. Complementary strategies for directing in vivo transcription factor binding through DNA binding domains and intrinsically disordered regions. Molecular Cell, 83(9):1462–1473.e5, May 2023. doi: 10.1016/j.molcel.2023.04.002. URL https://doi.org/10.1016/j.molcel.2023.04.002.

[20] Junji Iwahara, Markus Zweckstetter, and G. Marius Clore. Nmr structural and kinetic characterization of a homeodomain diffusing and hopping on nonspecific dna. Proceedings of the National Academy of Sciences, 103(41):15062–15067, October 2006. doi: 10.1073/pnas.0605868103. URL https://doi.org/10.1073/pnas.0605868103.

[21] A. Boija, I. A. Klein, B. R. Sabari, A. Dall'Agnese, E. L. Coffey, A. V. Zamudio, C. H. Li, K. Shrinivas, J. C. Manteiga, N. M. Hannett, et al. Transcription factors activate genes through the phase-separation capacity of their activation domains. Cell, 175:1842–1855, 2018. URL https://doi.org/10.1016/j.cell.2018.10.042.

[22] Michal Chappleboim, Segev Naveh-Tassa, Miri Carmi, Yaakov Levy, and Naama Barkai. Ordered and disordered regions of the origin recognition complex direct differential in vivo binding at distinct motif sequences. Nucleic Acids Research, 52(10):5720–5731, April 2024. ISSN 1362-4962. doi: 10.1093/nar/gkae249. URL http://dx.doi.org/10.1093/nar/gkae249.

[23] Otto G Berg, Robert B Winter, and Peter H Von Hippel. Diffusion-driven mechanisms of protein translocation on nucleic acids. 1. models and theory. Biochemistry, 20(24):6929–6948, 1981. URL https://doi.org/10.1021/bi00527a028.

[24] Otto G. Berg and Peter H. von Hippel. Selection of DNA binding sites by regulatory proteins. Journal of Molecular Biology, 193(4):723–743, February 1987. doi: 10.1016/0022-2836(87)90354-8. URL https://doi.org/10.1016/0022-2836(87)90354-8.

[25] Michael Slutsky and Leonid A. Mirny. Kinetics of protein-DNA interaction: Facilitated target location in sequence-dependent potential. Biophysical Journal, 87(6):4021–4035, December 2004. doi: 10.1529/biophysj.104.050765. URL https://doi.org/10.1529/biophysj.104.050765.

[26] Leonid Mirny, Michael Slutsky, Zeba Wunderlich, Anahita Tafvizi, Jason Leith, and Andrej Kosmrlj. How a protein searches for its site on dna: the mechanism of facilitated diffusion. Journal of Physics A: Mathematical and Theoretical, 42(43):434013, 2009. URL https://doi.org/10.1088/1751-8113/42/43/434013.

[27] Gene-Wei Li, Otto G. Berg, and Johan Elf. Effects of macromolecular crowding and DNA looping on gene regulation kinetics. Nature Physics, 5(4):294–297, March 2009. URL https://doi.org/10.1038/nphys1222.

[28] Olivier Bénichou, Claude Loverdo, Michel Moreau, and Raphael Voituriez. Intermittent search strategies. Reviews of Modern Physics, 83(1):81, 2011. URL https://doi.org/10.1103/RevModPhys.83.81.

[29] M Sheinman, O Bénichou, Y Kafri, and R Voituriez. Classes of fast and specific search mechanisms for proteins on dna. Reports on Progress in Physics, 75(2):026601, 2012. URL https://doi.org/10.1088/0034-4885/75/2/026601.

[30] Petter Hammar, Prune Leroy, Anel Mahmutovic, Erik G Marklund, Otto G Berg, and Johan Elf. The lac repressor displays facilitated diffusion in living cells. Science, 336(6088):1595–1598, 2012. URL https://doi.org/10.1126/science.1221648.

[31] Iris Dror, Remo Rohs, and Yael Mandel-Gutfreund. How motif environment influences transcription factor search dynamics: Finding a needle in a haystack. BioEssays, 38(7):605–612, May 2016. doi: 10.1002/bies.201600005. URL https://doi.org/10.1002/bies.201600005.

[32] Tamar Jana, Sagie Brodsky, and Naama Barkai. Speed–specificity trade-offs in the transcription factors search for their genomic binding sites. Trends in Genetics, 37(5):421–432, 2021. URL https://doi.org/10.1016/j.tig.2020.12.001.

[33] Kaustubh Wagh, Diana A. Stavreva, Arpita Upadhyaya, and Gordon L. Hager. Transcription factor dynamics: One molecule at a time. Annual Review of Cell and Developmental Biology, 39(1), August 2023. doi: 10.1146/annurev-cellbio-022823-013847. URL https://doi.org/10.1146/annurev-cellbio-022823-013847.

[34] C. Danilowicz, Y. Kafri, R. S. Conroy, V. W. Coljee, J. Weeks, and M. Prentiss. Measurement of the phase diagram of DNA unzipping in the temperature-force plane. Physical Review Letters, 93(7), August 2004. doi: 10.1103/physrevlett.93.078101. URL https://doi.org/10.1103/physrevlett.93.078101.

[35] Prince E Rouse Jr. A theory of the linear viscoelastic properties of dilute solutions of coiling polymers. The Journal of Chemical Physics, 21(7):1272–1280, 1953. URL https://doi.org/10.1063/1.1699180.

[36] Masao Doi and Samuel Frederick Edwards. The Theory of Polymer Dynamics, Oxford University Press, 1988. URL https://doi.org/.

[37] Nobuo Shimamoto. One-dimensional diffusion of proteins along dna: its biological and chemical significance revealed by single-molecule measurements. Journal of Biological Chemistry, 274(22):15293–15296, 1999. URL https://doi.org/10.1074/jbc.274.22.15293.

[38] Tao Hu and B. I. Shklovskii. Kinetics of viral self-assembly: Role of the single-stranded RNA antenna. Physical Review E, 75(5), May 2007. doi: 10.1103/physreve.75.051901. URL https://doi.org/10.1103/physreve.75.051901.

[39] Milagros Castellanos, Nivin Mothi, and Victor Muñoz. Eukaryotic transcription factors can track and control their target genes using DNA antennas. Nature Communications, 11(1), January 2020. URL https://doi.org/10.1038/s41467-019-14217-8.

[40] Felix Jonas, Miri Carmi, Beniamin Krupkin, Joseph Steinberger, Sagie Brodsky, Tamar Jana, and Naama Barkai. The molecular grammar of protein disorder guiding genome-binding locations. Nucleic Acids Research, 51(10):4831–4844, March 2023. ISSN 1362-4962. doi: 10.1093/nar/gkad184. URL http://dx.doi.org/10.1093/nar/gkad184.

[41] Vladimir Mindel, Sagie Brodsky, Aileen Cohen, Wajd Manadre, Felix Jonas, Miri Carmi, and Naama Barkai. Intrinsically disordered regions of the msn2 transcription factor encode multiple functions using interwoven sequence grammars. Nucleic Acids Research, 52(5):2260–2272, December 2023. ISSN 1362-4962. doi: 10.1093/nar/gkad1191. URL http://dx.doi.org/10.1093/nar/gkad1191.

[42] Amir Marcovitz and Yaakov Levy. Weak frustration regulates sliding and binding kinetics on rugged protein–dna landscapes. The Journal of Physical Chemistry B, 117(42):13005–13014, 2013. URL https://doi.org/10.1021/jp402296d.

[43] PG De Gennes and L Leger. Dynamics of entangled polymer chains. Annual Review of Physical Chemistry, 33(1):49–61, 1982. URL https://doi.org/10.1146/annurev.pc.33.100182.000405.

[44] Howard C Berg and Edward M Purcell. Physics of chemoreception. Biophysical journal, 20(2):193–219, 1977. URL https://doi.org/10.1016/S0006-3495(77)85544-6.

[45] Howard C Berg. Random walks in biology. In Random Walks in Biology. Princeton University Press, 2018. URL https://doi.org/.

[46] Sébastien Guilbaud, Laurence Salomé, Nicolas Destainville, Manoel Manghi, and Catherine Tardin. Dependence of DNA persistence length on ionic strength and ion type. Physical Review Letters, 122(2), January 2019. doi: 10.1103/physrevlett.122.028102. URL https://doi.org/10.1103/physrevlett.122.028102.

[47] Daniel R. Larson, Daniel Zenklusen, Bin Wu, Jeffrey A. Chao, and Robert H. Singer. Real-time observation of transcription initiation and elongation on an endogenous yeast gene. Science, 332(6028):475–478, April 2011. ISSN 1095-9203. doi: 10.1126/science.1202142. URL http://dx.doi.org/10.1126/science.1202142.

[48] J. J. Hopfield. Kinetic proofreading: A new mechanism for reducing errors in biosynthetic processes requiring high specificity. Proceedings of the National Academy of Sciences, 71(10):4135–4139, October 1974. ISSN 1091-6490. doi: 10.1073/pnas.71.10.4135. URL http://dx.doi.org/10.1073/pnas.71.10.4135.

[49] Emil Marklund, Guanzhong Mao, Jinwen Yuan, Spartak Zikrin, Eldar Abdurakhmanov, Sebastian Deindl, and Johan Elf. Sequence specificity in dna binding is mainly governed by association. Science, 375(6579):442–445, January 2022. ISSN 1095-9203. doi: 10.1126/science.abg7427. URL http://dx.doi.org/10.1126/science.abg7427.

[50] Gabriel E. Zentner, Sivakanthan Kasinathan, Beibei Xin, Remo Rohs, and Steven Henikoff. ChEC-seq kinetics discriminates transcription factor binding sites by DNA sequence and shape in vivo. Nature Communications, 6(1), October 2015. URL https://doi.org/10.1038/ncomms9733.

[51] Debora Tenenbaum, Koe Inlow, Larry J. Friedman, Anthony Cai, Jeff Gelles, and Jane Kondev. Rna polymerase sliding on dna can couple the transcription of nearby bacterial operons. Proceedings of the National Academy of Sciences, 120(30), July 2023. ISSN 1091-6490. doi: 10.1073/pnas.2301402120. URL http://dx.doi.org/10.1073/pnas.2301402120.

[52] Tal Einav, Shahrzad Yazdi, Aaron Coey, Pamela J. Bjorkman, and Rob Phillips. Harnessing avidity: Quantifying the entropic and energetic effects of linker length and rigidity for multivalent binding of antibodies to hiv-1. Cell Systems, 9(5):466–474.e7, November 2019. ISSN 2405-4712. doi: 10.1016/j.cels.2019.09.007. URL http://dx.doi.org/10.1016/j.cels.2019.09.007.

[53] E. Morgunova and J. Taipale. Structural perspective of cooperative transcription factor binding. Current Opinion in Structural Biology, 47:1–8, 2017. URL https://doi.org/10.1016/j.sbi.2017.03.006.

[54] B. R. Sabari, A. Dall'Agnese, A. Boija, I. A. Klein, E. L. Coffey, K. Shrinivas, B. J. Abraham, N. M. Hannett, A. V. Zamudio, J. C. Manteiga, et al. Coactivator condensation at super-enhancers links phase separation and gene control. Science, 361:eaar3958, 2018. URL https://doi.org/10.1126/science.aar3958.

[55] Samantha Kent, Kyle Brown, Chou-hsun Yang, Njood Alsaihati, Christina Tian, Haobin Wang, and Xiaojun Ren. Phase-separated transcriptional condensates accelerate target-search process revealed by live-cell single-molecule imaging. Cell Reports, 33(2):108248, October 2020. ISSN 2211-1247. doi: 10.1016/j.celrep.2020.108248. URL http://dx.doi.org/10.1016/j.celrep.2020.108248.

[56] Alex S. Holehouse and Birthe B. Kragelund. The molecular basis for cellular function of intrinsically disordered protein regions. Nature Reviews Molecular Cell Biology, 25(3):187–211, November 2023. ISSN 1471-0080. doi: 10.1038/s41580-023-00673-0. URL http://dx.doi.org/10.1038/s41580-023-00673-0.

[57] John D. Weeks, David Chandler, and Hans C. Andersen. Role of repulsive forces in determining the equilibrium structure of simple liquids. The Journal of Chemical Physics, 54(12):5237–5247, June 1971. doi: 10.1063/1.1674820. URL https://doi.org/10.1063/1.1674820.

[58] Ludovic Berthier and Giulio Biroli. Theoretical perspective on the glass transition and amorphous materials. Reviews of Modern Physics, 83(2):587–645, June 2011. doi: 10.1103/revmodphys.83.587. URL https://doi.org/10.1103/revmodphys.83.587.

[59] Zeba Wunderlich and Leonid A. Mirny. Spatial effects on the speed and reliability of protein–DNA search. Nucleic Acids Research, 36(11):3570–3578, May 2008. URL https://doi.org/10.1093/nar/gkn173.

[60] Ori Hachmo and Ariel Amir. Conditional probability as found in nature: Facilitated diffusion. American Journal of Physics, 91(8):653–658, August 2023. doi: 10.1119/5.0123866. URL https://doi.org/10.1119/5.0123866.

[61] Tao Hu, A. Yu. Grosberg, and B.I. Shklovskii. How proteins search for their specific sites on DNA: The role of DNA conformation. Biophysical Journal, 90(8):2731–2744, April 2006. doi: 10.1529/biophysj.105.078162. URL https://doi.org/10.1529/biophysj.105.078162.

[62] Joshua N. Milstein and Jens-Christian Meiners. Worm-Like Chain (WLC) Model, page 2757–2760. Springer Berlin Heidelberg, 2013. doi: 10.1007/978-3-642-16712-6_502. URL http://dx.doi.org/10.1007/978-3-642-16712-6_502.

[63] Ariel Afek, Joshua L. Schipper, John Horton, Raluca Gordân, and David B. Lukatsky. Protein−dna binding in the absence of specific base-pair recognition. Proceedings of the National Academy of Sciences, 111(48): 17140–17145, October 2014. ISSN 1091-6490. doi: 10.1073/pnas.1410569111. URL http://dx.doi.org/10.1073/pnas.1410569111.

Supplementary Materials: Design principles of transcription factors with intrinsically disordered regions

Contents

S1. Broad applicability of probability density $f(r, l)$ 18

S2. Derivation of the binding probability 19

S3. Q varying with l_0/d for all combinations of n_b and n_t 21

S4. P_{TF} varying with n_b and n_t 22

S5. Robustness of the relationships: $n_b^* \sim n_t^*$ and n_b^* decreases with increasing E_B 23

S6. Robustness of the binding design principles 24

S7. TF walking along the antenna once it attaches, and t_{total} vs. E_B and vs. $\tilde{n}$ 25

S8. A single round of 3D-1D search is typically the case in the optimal search process. 27

S9. Robustness of mean total search time with changing the antenna geometry 29

S10. 3D diffusion coefficients in a complex DNA configuration 30

S11. Properties of the octopusing walk 31

S1. Broad applicability of probability density $f(r, l)$

We verify the broad applicability of Eq. [1] in the main text, regardless of the specific details of microscopic interactions. To demonstrate this, we only require that the density function of the end-to-end distance r for a segment containing m amino acids (AAs), denoted as $f(r, l_0)$, complies with Eq. [1]. Specifically, it is.

$$f(r, l_0) \approx \left(\frac{3}{2\pi l_0^2}\right)^{3/2} \exp\left(-\frac{3r^2}{2l_0^2}\right), \tag{S1}$$

where l_0 is the typical length of the segment. When m is large, according to the central limit theorem, r should conform to the distribution in Eq. [S1] with a variance of $l_0^2 = m a_{\text{eff}}^2$, where a_{eff} represents the effective length of an individual AA.

Next, we will consider a specific form of interaction, of springs with a finite rest-length. In one limit (where the rest length vanishes), this corresponds to the Rouse model (where Eq. [S1] is exact for any value of m, not only asymptotically) and in another limit (where the springs are very stiff) this corresponds to a chain of rods. As we shall see, Eq. [S1] provides an excellent approximation already for moderate values of m.

To proceed, we consider two adjacent AAs at positions $\vec{r}_i$ and $\vec{r}_{i+1}$ with an interaction denoted by $u(|\vec{r}_i - \vec{r}_{i+1}|)$. Their probability density is $\rho(\vec{r}_i, \vec{r}_{i+1}) \propto \exp\left(-u(|\vec{r}_i - \vec{r}_{i+1}|)/(k_B T)\right)$. a_{eff}^2 can be calculated using $\rho(\vec{r}_i, \vec{r}_{i+1})$:

$$a_{\text{eff}}^2 = \int d\vec{r} \int d\vec{r}_i \int d\vec{r}_{i+1}\, |\vec{r}_i - \vec{r}_{i+1}|^2 \rho(\vec{r}_i, \vec{r}_{i+1}) \delta\left(\vec{r} - (\vec{r}_i - \vec{r}_{i+1})\right). \tag{S2}$$

Specifically, for a spring-like interaction with a stiffness constant k_0 and a rest length b_0, the interaction is given by $u = \frac{1}{2} k_0 \left(|\vec{r}_i - \vec{r}_{i+1}| - b_0\right)^2$. This formula can also be interpreted as a harmonic approximation of the interaction around the equilibrium distance b_0. In this case, a_{eff}^2 is derived analytically:

$$a_{\text{eff}}^2 = a_0^2 + b_0^2 + \frac{2b_0^2 a_0^2}{a_0^2 + 3b_0^2}\left(1 + \frac{2a_0^3}{6b_0^2 a_0 + \sqrt{6\pi} b_0 \left(a_0^2 + 3b_0^2\right)\left(1 + \text{Erf}\left(\sqrt{\frac{3}{2}}\frac{b_0}{a_0}\right)\right)\exp\left(\frac{3b_0^2}{2a_0^2}\right)}\right), \tag{S3}$$

where $a_0^2 \equiv 3k_0/k_B T$ and $\text{Erf}(z) = \frac{2}{\sqrt{\pi}} \int_0^z \exp(-x^2/2) dx$ is the error function. When $b_0 = 0$, we have $a_{\text{eff}} = a_0$, and Eq. [S1] holds for any m. When $b_0 \gg a_0$, then $a_{\text{eff}} \approx b_0$ corresponds to a chain of rods where the angle between consecutive rods is free to rotate. Fig. S1(a) shows that the numerical results obtained from this harmonic interaction are in good agreement with Eq. [S1] even at moderate values of m. The inset displays the variation of a_{eff}^2/a_0^2 with b_0/a_0 obtained from Eq. [S3]. In Fig. S1(b), with $b_0 = a_0$, $f(r, l_0)$ rapidly converges to Eq. [S1].

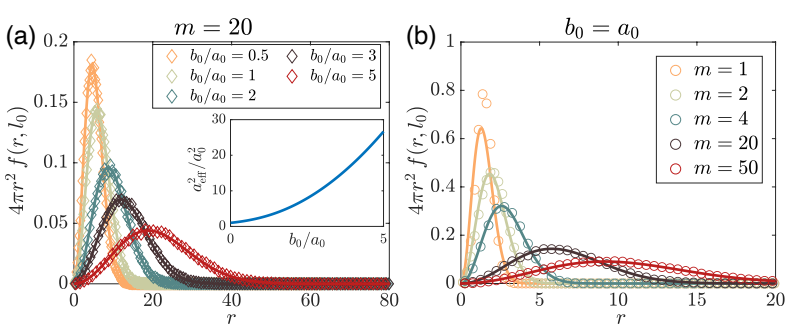

Figure S1: $f(r, l_0)$ aligns well with Eq. [S1] (solid curves) for moderate m at various b_0. Inset: a_{eff}^2/a_0^2 vs. b_0/a_0 from Eq. [S3]. (b) Eq. [S1] serves as a good approximation (solid lines) even at small m.

S2. Derivation of the binding probability

In this section, we derive the generalized binding probability P_{TF} for n_b IDR binding sites and n_t IDR targets. To achieve this generalization, we consider all the possible number of bindings, n from 0 to $\min(n_b, n_t)$, and all possibilities for binding orientations for each n. Note that the energy and entropy trade-off is naturally included in our model, and the generalized formula of P_{TF} is also applicable for non-uniformly distributed binding targets and binding sites.

Based on the Rouse model, the system's energy can be expressed as $\frac{k}{2}\sum_{i=1}^{n_b}(\vec{r}_i-\vec{r}_{i-1})^2 = \frac{3k_BT}{2l_0^2}\sum_{i=1}^{n_b}(\vec{r}_i-\vec{r}_{i-1})^2$, where $\vec{r}_i$ represents the position of the binding site i. The probability density in the absence of binding reads:

$$\rho(\vec{r}_0,...,\vec{r}_{n_b}) = \frac{1}{V_c}\left(\frac{3}{2\pi l_0^2}\right)^{\frac{3}{2}n_b} e^{-\frac{3}{2l_0^2}\sum_{i=1}^{n_b}(\vec{r}_i-\vec{r}_{i-1})^2}, \tag{S4}$$

where $\int d^3\vec{r}_0 ... \int d^3\vec{r}_{n_b}\rho(\vec{r}_0,...,\vec{r}_{n_b}) = 1$.

Now we consider a given configuration with n IDR sites bound, where IDR sites $q_1 < ... < q_n$ are bound to targets $s_1, ..., s_n$. The positions of these bound targets are at $\vec{R}_{s_1}, ..., \vec{R}_{s_n}$. The DBD site is denoted by $q_0 = 0$ and its target is denoted by $s_0 = 0$. There are $n_b - n$ unbound IDR sites, indicated by $\bar{q}_1 < ... < \bar{q}_{n_b-n}$. The corresponding binding probability is given by:

$$P_{\mathrm{bound}}(\mathrm{orn}, n) = \frac{1}{Z}\prod_{i=0}^{n}\int_{\vec{r}_{q_i}\in V_1} d^3\vec{r}_{q_i}\prod_{\ell=1}^{n_b-n}\int_{\vec{r}_{\bar{q}_\ell}\notin V_1} d^3\vec{r}_{\bar{q}_\ell}\rho(\vec{r}_0,...,\vec{r}_{n_b})\, e^{E_{\mathrm{DBD}}+nE_B}, \tag{S5}$$

where "orn" stands for the orientation of the given configuration, Z is the normalization factor, and E_{DBD} is the DBD site binding energy for its target. There are $\binom{n_b}{n}\binom{n_t}{n}n!$ possible binding orientations at n. The key insight in evaluating this integral is to realize that we can use the result of Eq. [1] of the main text to integrate out the degrees of freedom associated with the sites between q_{i-1} and q_i:

$$\prod_{\bar{q}_\ell=q_{i-1}+1}^{q_i-1}\left[\int d^3\vec{r}_{\bar{q}_\ell}\left(\frac{3}{2\pi l_0^2}\right)^{3/2}\exp\left(-\frac{3(\vec{r}_{\bar{q}_\ell}-\vec{r}_{\bar{q}_\ell-1})^2}{2l_0^2}\right)\right] = f\left(\left|\vec{r}_{q_i}-\vec{r}_{q_{i-1}}\right|, \sqrt{q_i-q_{i-1}}\,l_0\right). \tag{S6}$$

Since $r_{q_{i-1}}$ and r_{q_i} are confined to a very small volume V_1, to an excellent approximation we may simply evaluate $f\left(\left|\vec{r}_{q_i}-\vec{r}_{q_{i-1}}\right|, \sqrt{q_i-q_{i-1}}\,l_0\right)$ in Eq. [S6] at $\vec{r}_{q_{i-1}} = \vec{R}_{s_{i-1}}$ and $\vec{r}_{q_i} = \vec{R}_{s_i}$, to obtain:

$$P_{\mathrm{bound}}(\mathrm{orn}, n) \simeq \frac{1}{Z}\frac{V_1^{n+1}}{V_c}\prod_{i=1}^{n} f(|s_i-s_{i-1}|\,d, \sqrt{q_i-q_{i-1}}\,l_0)e^{E_{\mathrm{DBD}}+nE_B} = \frac{1}{Z}r_{\mathrm{DBD}}\prod_{i=1}^{n}\mathcal{P}(E_B, r_{\mathrm{orn},i}, l_{\mathrm{orn},i}), \tag{S7}$$

where $r_{\mathrm{DBD}} \equiv \frac{V_1}{V_c}e^{E_{\mathrm{DBD}}}$, $r_{\mathrm{orn},i} = |s_i - s_{i-1}|\,d$, $l_{\mathrm{orn},i} = \sqrt{q_i-q_{i-1}}\,l_0$, and $\mathcal{P}(E_B, r_{\mathrm{orn},i}, l_{\mathrm{orn},i}) = e^{E_B}V_1 f(r_{\mathrm{orn},i}, l_{\mathrm{orn},i})$.

To give a specific example, consider the binding topology corresponding to Fig. S2. In this case, $n = 3$, $l_{\mathrm{orn},1} = l_0$ (since there is one spring between the DBD and the first binding site), $l_{\mathrm{orn},2} = \sqrt{3}l_0$ (since there are 3 springs between q_1 and q_2) and similarly $l_{\mathrm{orn},3} = l_0$. Eq. [S6] implies that the contribution of this diagram to the binding probability is: $\frac{1}{Z}\frac{V_1^4}{V_c}\frac{27}{(2\pi l_0^2)^{9/2}}e^{3E_B+E_{\mathrm{DBD}}-5d^2/l_0^2}$. Note that while in this example, the order of the target sites is monotonic (i.e., as we increase the index of the binding sites, we progressively move further away from the DBD), in principle, we should sum over *all* diagrams, including those where the order is non-monotonic. At $n = 0$, $P_{\mathrm{bound}}(\mathrm{orn}, 0) = \frac{1}{Z}r_{\mathrm{DBD}}$.

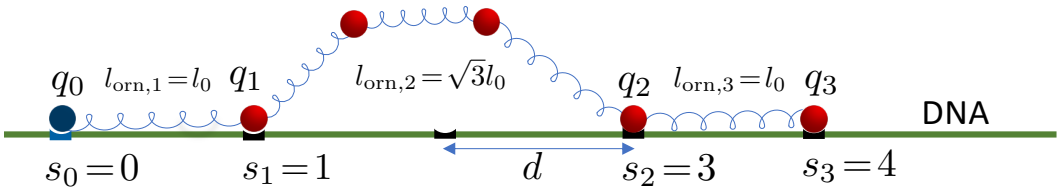

Figure S2: A diagram of the bound configurations at $n=3$.

Similarly, for the state where the DBD is unbound and $n \geq 2$ IDR sites are bound, the binding probability reads:

$$P_{\mathrm{unbound}}(\mathrm{orn}, n) = \frac{1}{Z}\int_{\vec{r}_0 \notin V_1} d^3\vec{r}_0 \prod_{\ell=1}^{n}\int_{\vec{r}_{q_\ell}\in V_1} d^3\vec{r}_{q_\ell} \prod_{\ell=1}^{n_b-n}\int_{\vec{r}_{\bar{q}_\ell}\notin V_1} d^3\vec{r}_{\bar{q}_\ell}\rho(\vec{r}_0,...,\vec{r}_{n_b})e^{nE_B} \tag{S8}$$

$$\simeq \frac{1}{Z} r_{\mathrm{IDR}} \prod_{i=2}^{n}\mathcal{P}(E_B, r_{\mathrm{orn},i}, l_{\mathrm{orn},i}), \tag{S9}$$

where $r_{\mathrm{IDR}} \equiv \frac{V_1}{V_c}e^{E_B}$. For $n=1$, $P_{\mathrm{unbound}}(\mathrm{orn},1) = \frac{n_t n_b}{Z} r_{\mathrm{IDR}}$. Here $n_t n_b$ represents the number of possibilities for one of the n_b IDR sites bound to one of the n_t targets. For $n=0$, $P_{\mathrm{unbound}}(\mathrm{orn},0) = \frac{1}{Z}\prod_{i=0}^{n_b}\int_{\vec{r}_i\notin V_1} d^3\vec{r}_i \rho(\vec{r}_0,...,\vec{r}_{n_b}) \simeq \frac{1}{Z}$.

Since the sum of all the possibilities is equal to 1, as given by: $\sum_{n=0}^{n_{\min}}\sum_{\mathrm{orn}}(P_{\mathrm{bound}}+P_{\mathrm{unbound}})=1$, where $n_{\min}=\min\{n_b, n_t\}$, we can determine the normalization factor. Therefore, the binding probability P_{TF} for the DBD bound in its target can be expressed as:

$$P_{\mathrm{TF}} = \frac{r_{\mathrm{DBD}}\left(1+\sum_{n=1}^{n_{\min}}\sum_{\mathrm{orn}}\prod_{i=1}^{n}\mathcal{P}(E_B, r_{\mathrm{orn},i}, l_{\mathrm{orn},i})\right)}{r_{\mathrm{DBD}}\left(1+\sum_{n=1}^{n_{\min}}\sum_{\mathrm{orn}}\prod_{i=1}^{n}\mathcal{P}(E_B, r_{\mathrm{orn},i}, l_{\mathrm{orn},i})\right)+1+r_{\mathrm{IDR}}\left(n_t n_b+\sum_{n=2}^{n_{\min}}\sum_{\mathrm{orn}}\prod_{i=2}^{n}\mathcal{P}(E_B, r_{\mathrm{orn},i}, l_{\mathrm{orn},i})\right)}. \tag{S10}$$

When $P_{\mathrm{TF}} \ll 1$, we can approximate P_{TF} as

$$P_{\mathrm{TF}} \approx \left(1+\sum_{n=1}^{n_{\min}}\sum_{\mathrm{orn}}\prod_{i=1}^{n}\mathcal{P}(E_B, r_{\mathrm{orn},i}, l_{\mathrm{orn},i})\right)P_{\mathrm{simple}}, \tag{S11}$$

where we have considered the facts that $r_{\mathrm{IDR}} < r_{\mathrm{DBD}}$ because $E_B < E_{\mathrm{DBD}}$, and $P_{\mathrm{simple}} = r_{\mathrm{DBD}}/(1+r_{\mathrm{DBD}}) \approx r_{\mathrm{DBD}}$ due to $r_{\mathrm{DBD}} \ll 1$. For instance, taking $E_{\mathrm{DBD}}=15$, $V_1 = 1\mathrm{bp}^3 \approx (0.34\mathrm{nm})^3$, and $V_c = 1\mu m^3$, we find that $r_{\mathrm{DBD}} \sim 10^{-4}$.

At $n_b = n_t = 1$, the generalized Eq. [S10] simplifies to the following expression:

$$P_{\mathrm{TF}} = \frac{r_{\mathrm{DBD}}\left[1+e^{E_B}V_1 f(d,l_0)\right]}{r_{\mathrm{DBD}}\left[1+e^{E_B}V_1 f(d,l_0)\right]+r_{\mathrm{IDR}}+1}. \tag{S12}$$

Therefore, P_{TF} can be approximated as $(1+\mathcal{P})P_{\mathrm{simple}}$, as illustrated in Eq. [6] of the main text. This approximation is also derivable from Eq. [S11].

S3. Q varying with l_0/d for all combinations of n_b and n_t

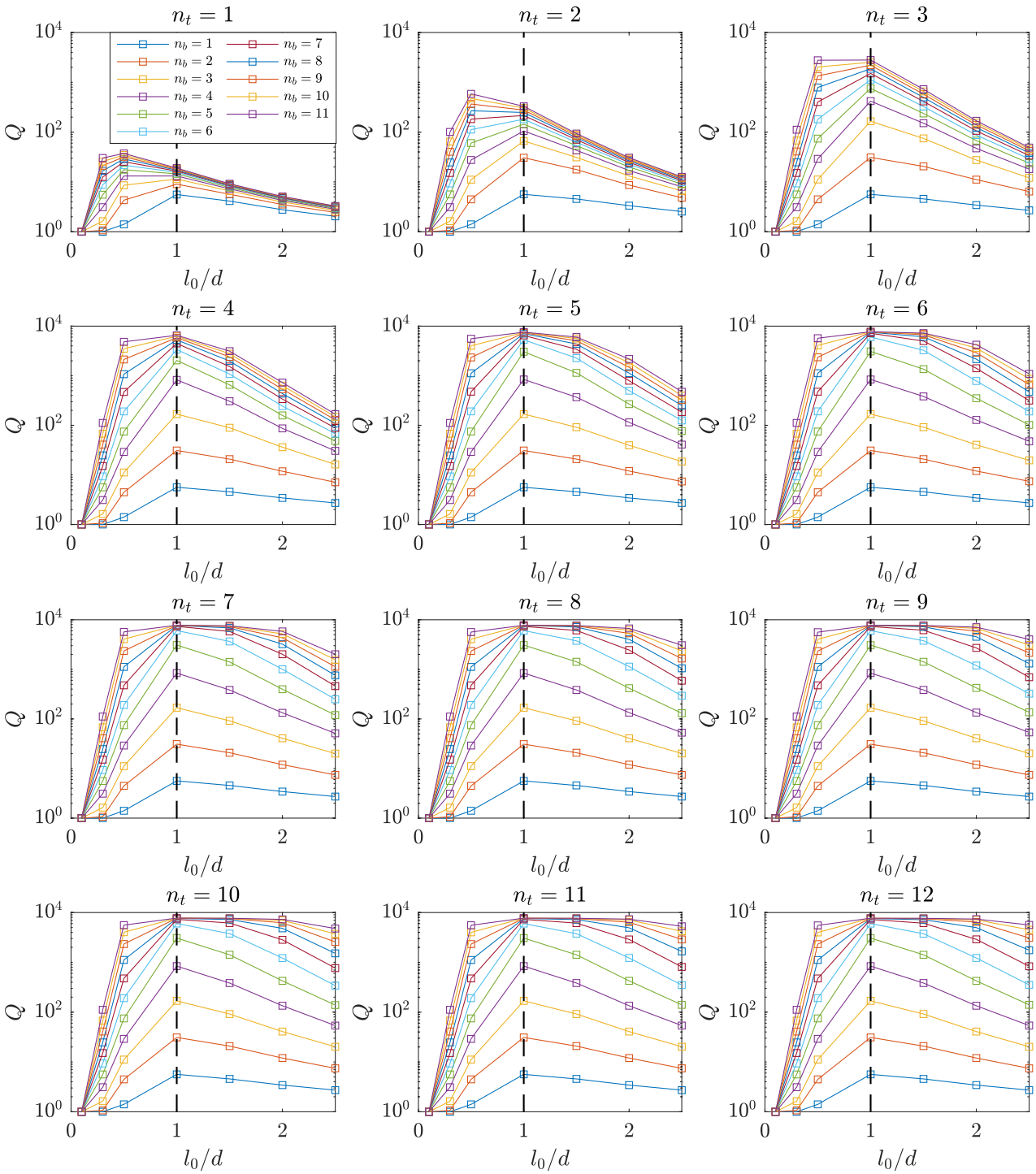

Figure S3: Maximal Q is observed at $l_0 \sim d$ for all combinations of n_b and n_t.

S4. P_{TF} varying with n_b and n_t

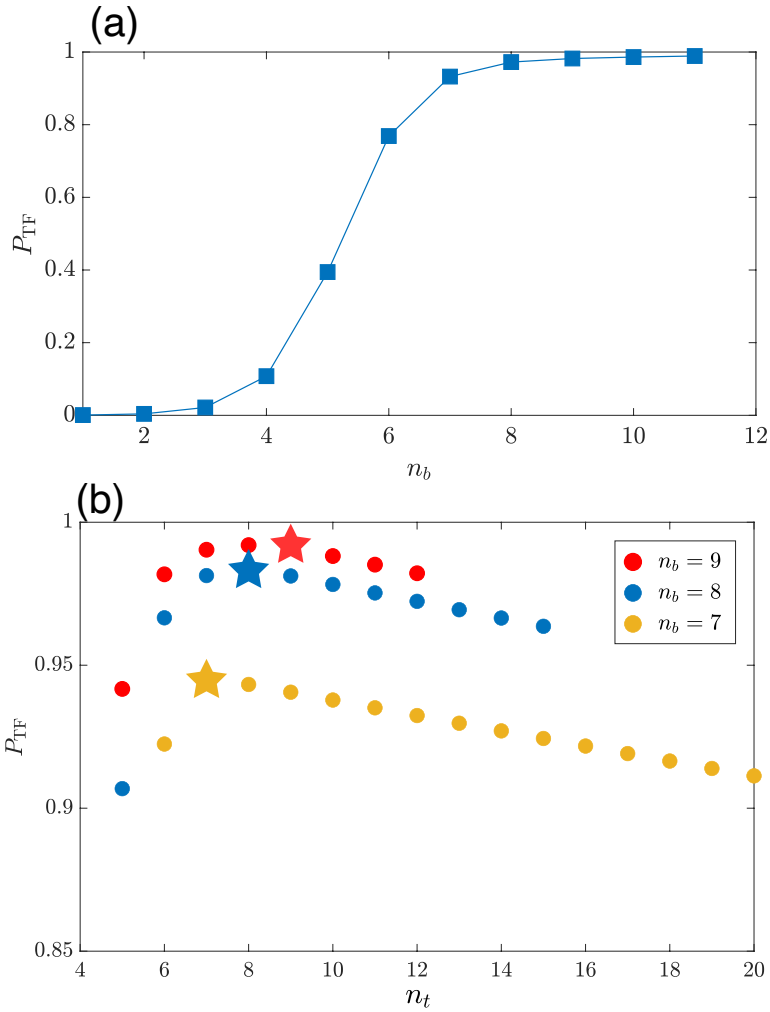

Figure S4: (a) P_{TF} varying with n_b at $n_t = 12$. P_{TF} initially increases rapidly, until eventually saturating. (b) P_{TF} varies non-monotonically with n_t. P_{TF} slightly decreases with increasing n_t at $n_t > n_b$. Three examples at $n_b = 7, 8, 9$ are displayed. P_{TF} is denoted by pentagrams at $n_t = n_b$.

S5. Robustness of the relationships: $n_b^* \sim n_t^*$ and n_b^* decreases with increasing E_B

Fig. S5 shows the contour lines at $P_{\mathrm{TF}} = 0.9$ and $P_{\mathrm{TF}} = 0.5$ for various E_B. All take an approximate symmetrical L-shape, indicating that for a given E_B, the optimal values n_b^* and n_t^* are comparable, as guided by the black dashed line $y = x$. As E_B increases, the contour lines shift towards lower values of n_b and n_t, indicating a decrease in n_b^* as E_B increases.

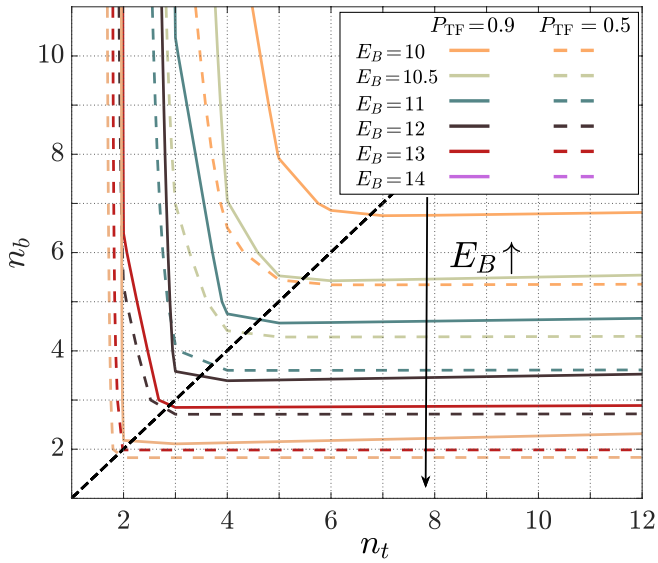

Figure S5: Contour lines at $P_{\mathrm{TF}} = 0.9$ and $P_{\mathrm{TF}} = 0.5$ on the plane defined by the number of binding sites, n_b, and the number of binding targets, n_t. The black dashed line is added to guide the relationship $n_b = n_t$.

S6. Robustness of the binding design principles

In the main text, we employed uniform binding site distances in TFs, represented as l_0, and uniform binding target distances on the DNA, denoted as d, to obtain the design principles. Here, we also explore the scenario where both IDR binding sites and their targets are distributed as a Poisson process (i.e., the distance between neighboring sites is exponentially distributed), with mean values of l_0 and d, respectively. Figure S6 is similar to Figure 2 in the main text. We observe that the design principles identified in the main text are applicable under these conditions as well.

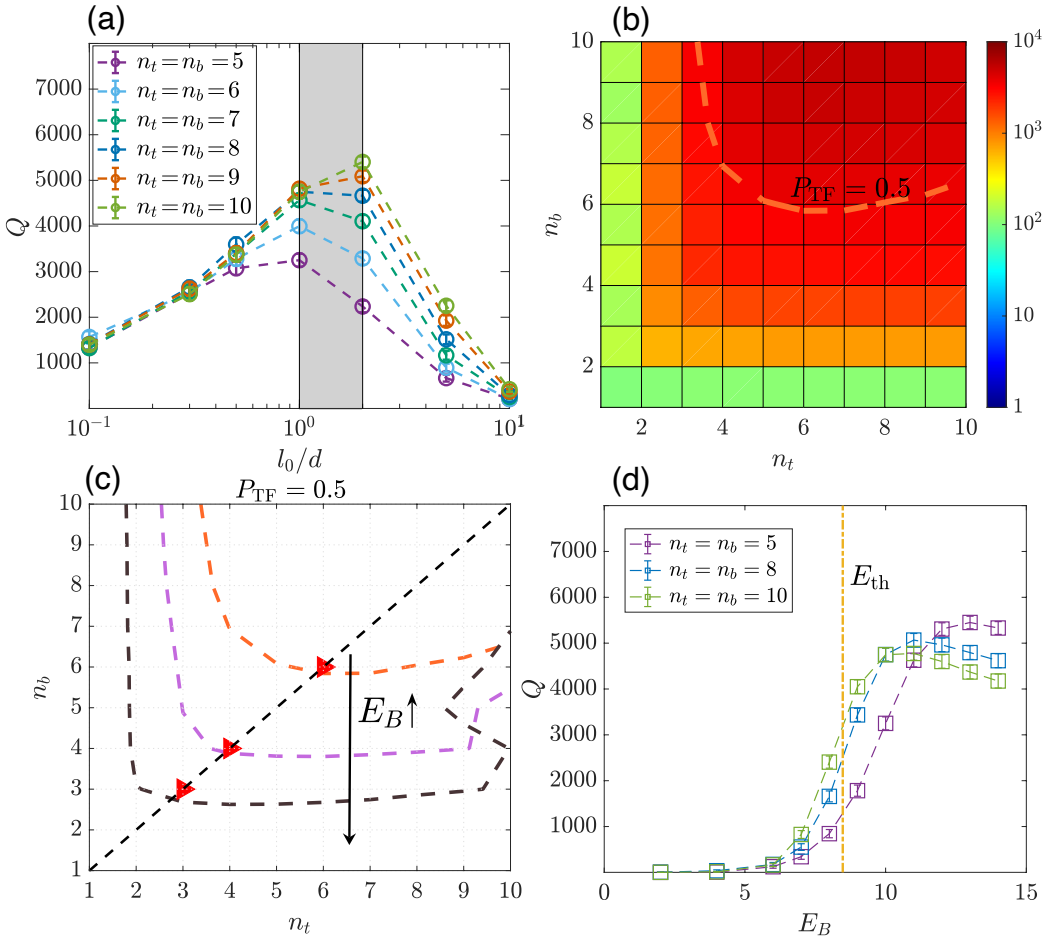

Figure S6: Plots of the affinity enhancement, quantified by the ratio $Q \equiv P_{\rm TF}/P_{\rm simple}$, for the case where IDR sites as well as their targets are randomly positioned on the IDR and DNA, respectively. See the analogous Figure 2 in the main text for the case of homogeneously distributed IDR sites and targets. (a) Q is maximal when $l_0 \sim d$ (shaded region) for different values of $n_t = n_b$. The average distance between IDR sites is l_0, and the average distance between IDR targets is d. (b) A heatmap of Q at $E_B = 10$ and $l_0 = d$. (c) Contour lines at different E_B at $P_{\rm TF} = 0.5$ exhibit an approximate symmetrical L-shape, which indicates $n_b^* = n_t^*$, as shown by the red triangles. n_b^* decreases with increasing E_B. (d) Q varies with E_B for several different constants of $n_t = n_b$. The characteristic energy $E_{\rm th}$, as predicted by Eq. [5] in the main text, corresponds to the region where a notable increase is observed.

S7. TF walking along the antenna once it attaches, and t_{total} vs. E_B and vs. $\tilde{n}$

We show a typical example of the trajectory of a TF (red) in the cell nucleus (light blue) in Fig. S7(a) where the TF walks along the antenna to the DBD target once it attaches the IDR targets at $\tilde{n}^*$ and E_B^*. The DBD target is at the origin. In Fig. S7(b), we find that the average number of rounds the TF hits the antenna, n_{hits}, is close to 1, so it is fair to describe the overall search process as two distinct steps with the first step being purely a 3D search and the second a purely 1D search. This is expressed by Eq. [5] in the main text.

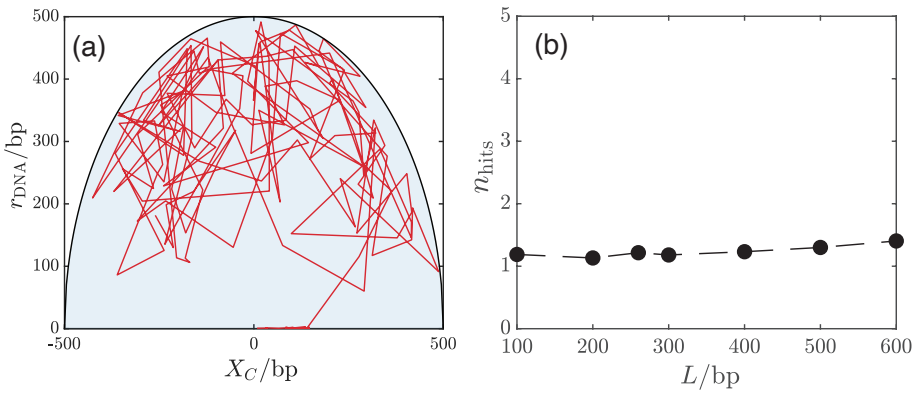

Figure S7: (a) A trajectory (red) of TF in the cell nucleus (light blue). r_{DNA} is the average distance of the TF to the antenna, and X_c is the position of the center of mass along the antenna direction. The trajectory is displayed with a time interval of $10^6 t_0$. (b) The average number of rounds the TF hits the antenna, n_{hits}, before reaching the DBD target. The optimal mean total search time is obtained at $L^* = 300\text{bp}$.

The minimal search time, t_{min}, is obtained at L^*, E_B^*, and $\tilde{n}^*$. Fig. S8(a) shows t_{total} vs. E_B at fixed L^* and $\tilde{n}^*$. When $E_B > E_B^*$, t_{3D} does not depend on E_B as we predict (red solid line) and t_{1D} exponentially increases with increasing E_B. The solid blue line shows the exponential dependence of t_{1D} on E_B, also shown in the inset. When $E_B < E_B^*$, the number of rounds of hits on the antenna, n_{hits}, is larger than 1, as displayed in the inset. In this scenario, equation (5) in the main text becomes ineffective, resulting in a significantly longer search time than t_{min}.

Fig. S8(b) shows t_{total} vs. $\tilde{n}$ at fixed $L^*$and E_B^*. When $\tilde{n} > \tilde{n}^*$, t_{3D} and t_{1D} agree with the prediction of Eq. [5] (red curve and blue curve). Interestingly, we find that t_{1D} only weakly depends on $\tilde{n}$. This arises due to the compensating effects of attaching and detaching: As $\tilde{n}$ increases, the TF attaches to new targets more easily, speeding up 1D motion. However, it also makes detaching from the current site more difficult, thereby slowing down 1D motion. When $\tilde{n} < \tilde{n}^*$, Eq. [5] breaks down because of multiple rounds of hits, which is verified in the inset. As a result, both t_{total} and t_{3D} increases with decreasing $\tilde{n}$, leading them to become significantly longer than t_{min}. If each round of 3D search is independent, the 3D search time should be n_{hits} times the one round of 3D search time, displayed in the black curve.

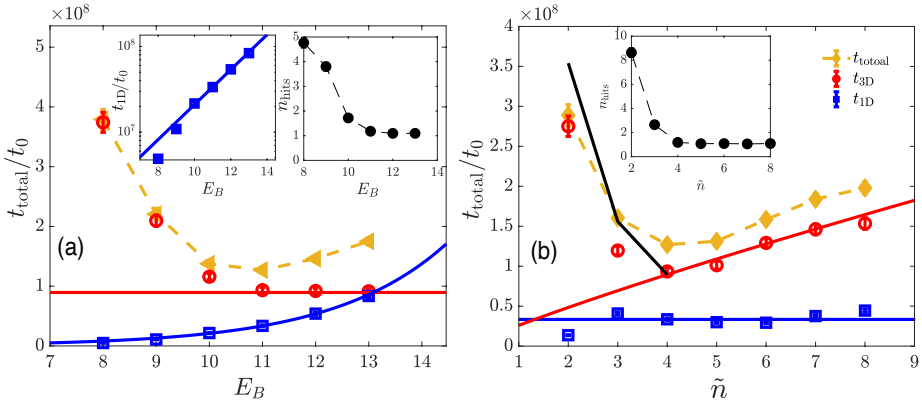

Figure S8: (a) t_{total}, t_{3D}, and t_{1D} vs. E_B at fixed L^* and $\tilde{n}^*$. The red solid line is the prediction of t_{3D} from Eq. [5], and the blue line (also in the inset) is the exponential fit for t_{1D}. The black curve in the inset is the number of rounds the TF hits the antenna, n_{hits}, vs. E_B. (b) t_{total}, t_{3D}, and t_{1D} vs. $\tilde{n}$ at fixed L^* and E_B^*. The red and blue solid lines represent the predictions of t_{3D} and t_{1D} from Eq. [5], respectively. n_{hits} varying with $\tilde{n}$ is shown in the inset.

S8. A single round of 3D-1D search is typically the case in the optimal search process.

In this section, we will show that the optimal search process (i.e., minimizing the mean first passage time) generically takes place via a single round of 3D-1D search. To do so, we first need to derive the expression for the mean total search time, t_{total}, and its dependence on the relevant parameters, including, importantly, E_B and L. According to our model presented in the main text: A TF is initially in the 3D nucleus space; it can attach to the antenna and perform 1D diffusion with the coefficient denoted by D_1. We assume the DBD target is placed in the middle of the antenna, as shown in Fig. 1 of the main text. The mean search time taken for a TF to move from 3D space and attach to the antenna is denoted by $t_{3\text{D}}$. The TF can also detach from the antenna at a rate we denote by Γ, perform a 3D random walk, until ultimately attaching again to the antenna. In the following, we will make the assumption (often made in the context of FD model [23–29]) that the binding position after such a 3D excursion is uniformly distributed on the antenna. Both D_1 and Γ are functions of E_B. When the TF is on the antenna, its mean search time to reach the DBD target, located a distance x away on the antenna, is represented by $\mathcal{T}(x)$. Naturally, $\mathcal{T}(x)$ is zero when $x = 0$, the location of the DBD target. The mean total search time t_{total} is thus given by

$$t_{\text{total}} = \frac{1}{L}\int_{-L/2}^{L/2} \mathcal{T}(x)dx + t_{3\text{D}}. \tag{S13}$$

Consider a time interval Δt. With probability $\Gamma\Delta t$ the TF falls off and the mean first passage time to reach the target is $t_{\text{total}} + \Delta t$. Otherwise, with probability $1 - \Gamma\Delta t$, the mean first passage time would be the average of the two possible outcomes, namely, $(\mathcal{T}(x+\Delta x) + \mathcal{T}(x-\Delta x))/2 + \Delta t$. This recursive reasoning leads us to the following equation:

$$\mathcal{T}(x) = \Delta t + \frac{\mathcal{T}(x-\Delta x) + \mathcal{T}(x+\Delta x)}{2}(1-\Gamma\Delta t) + t_{\text{total}}\Gamma\Delta t. \tag{S14}$$

In the continuous limit, we have

$$D_1\frac{\partial^2\mathcal{T}(x)}{\partial x^2} - \Gamma\mathcal{T}(x) + \Gamma t_{\text{total}} + 1 = 0, \tag{S15}$$

where $D_1 \equiv (\Delta x)^2/(2\Delta t)$. By applying the boundary conditions, specifically the absorbing boundary condition at $x = 0$ and the reflecting boundary conditions at $x = \pm L/2$, $\mathcal{T}(x)$ is determined as

$$\mathcal{T}(x) = \left(t_{\text{total}} + \Gamma^{-1}\right)\left[1 - \frac{\cosh(\frac{L-2|x|}{L_s})}{\cosh(\frac{L}{L_s})}\right], \tag{S16}$$

where L_s, representing the 1D diffusion distance, is defined by $L_s \equiv 2\sqrt{D_1\Gamma^{-1}}$ [59]. Therefore, t_{total} can be self-consistently solved by substituting $\mathcal{T}(x)$ into Eq. [S13], presented as follows:

$$t_{\text{total}} = \frac{L}{L_s}\coth\left(\frac{L}{L_s}\right)t_{3\text{D}} + \left[\frac{L}{L_s}\coth\left(\frac{L}{L_s}\right) - 1\right]\Gamma^{-1}. \tag{S17}$$

We can obtain t_{total} in two limiting cases:

- When $L \gg L_s$, where multiple rounds of 3D-1D excursions are needed to find the target, we have $t_{\text{total}} = \frac{L}{L_s}\left(t_{3\text{D}} + \Gamma^{-1}\right)$. This is the same as the results of the facilitated diffusion model [28, 29, 59, 60].
- When $L \ll L_s$, where a single round of 3D-1D search can find the target, we get $t_{\text{total}} = t_{3\text{D}} + \frac{L^2}{12D_1}$. This matches Eq. [5] in the main text when $L < 2R$.

Note that the calculations above did not assume an optimal or efficient search process, but simply characterized the dependence of the mean first passage time on the model parameters. Next, based on the expression for t_{total} in Eq. [S17], we will prove that the search process involving multiple rounds of 3D-1D search is *not* optimal. This conclusion is reached by showing that the minimum t_{total} always occurs in the regime where $L < 2L_s$ (since L_s is the typical distance covered by 1D diffusion on the antenna before falling off, and the maximal distance needed to be traversed on the antenna is $L/2$). We emphasize an important distinction between our model and the well-studied facilitated diffusion model (where it is established that *multiple* rounds of search are needed for efficient search): in our case the antenna length L is a *variable* that can be optimized over (since we assume evolution has optimized over the size of the region flanking the DBD in which binding sites for the IDR are located). In the facilitated diffusion model, L is assumed to be the length of the genome, since the interactions of the TF and the DNA are assumed non-specific.

To proceed, let us first note that the factor $\coth\left(\frac{L}{L_s}\right)$ in Eq. [S17] quickly converges to 1 as the ratio of L/L_s increases. For instance, when the ratio is 2, we have $\coth(2) \approx 1.04$. Thus, for $L > 2L_s$, we could approximate t_{total} as

$$t_{\text{total}} \approx \frac{L}{L_s} t_{\text{3D}} + \left(\frac{L}{L_s} - 1\right) \Gamma^{-1}. \tag{S18}$$

Then, we consider how t_{3D} varies with L. If the rate to hit the antenna after 3D diffusion was the sum of the rates to hit every infinitesimal segment of it, we would expect the rate to hit the antenna to be *linear* in L, and the mean first passage time to scale as $1/L$. However, these processes are not uncorrelated. Interestingly, when $L < 2R$, and assuming a straight antenna, t_{3D} is proportional to $\ln(L)/L$ (see Eq. [5] in the main text), implying that for a straight antenna the effect of these correlations is mild. However, when $L > 2R$, the antenna is curved rather than straight (due to the limitations imposed on the DNA conformation by the dimensions of the nucleus), and the dependence of t_{3D} on L is weaker [61]. Thus, for any given L greater than $2L_s$, t_{3D} varies more weakly than $1/L$, making the first term of t_{total} in Eq. [S18] an increasing function of L. Clearly, the second term increases as well. Therefore, when $L > 2L_s$, regardless of the functional forms of D_1 and Γ^{-1} on E_B, t_{total} decreases with decreasing L. Thus, the minimum t_{total} occurs in the regime where $L < 2L_s$, and the optimal search typically consists of a single search round.

S9. Robustness of mean total search time with changing the antenna geometry

We checked that the mean total search time (Mean First Passage Time) for IDR targets, generated via the worm-like chain model – a random walk with a persistence length [62], does not significantly differ from the scenario where targets are arranged linearly, as presented in the main text. See Fig. S9 for details.

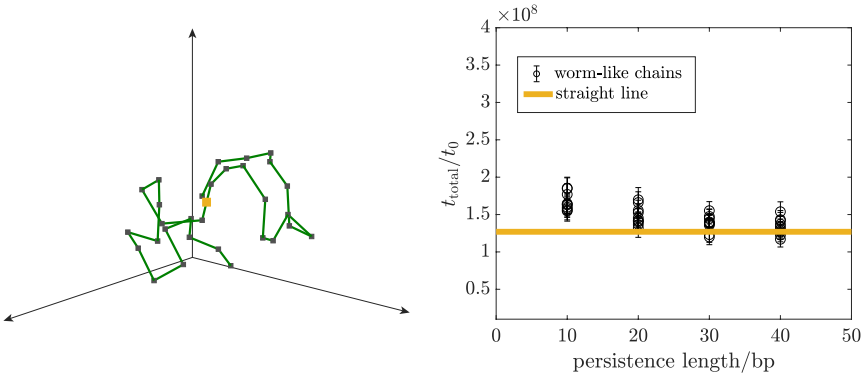

Figure S9: Left: an example of the target configuration (the antenna) generated by the worm-like chain model, where $L = 300$bp, $d = 10$bp, and the persistence length also equals 10bp. Right: Mean total search times weakly vary with persistence length when targets are generated using the worm-like chain model. The values are represented by the black dots, with parameters set to $E_B = 11$, $L = 300$ bp, and $\tilde{n} = 4$. For each persistence length, we obtained ten mean total search times by considering ten different target configurations. The mean total search times do not exhibit significant differences compared to that for targets arranged linearly (indicated by the horizontal orange line).

S10. MSD in a complex DNA configuration

In Fig. S10, we run simulations to examine how the Mean Square Displacement (MSD) of a point searcher is influenced by the binding energy (E_{nonsp}) between the TF and the entire DNA in a complex DNA configuration. Fig. S10(a) shows the DNA configuration generated via the worm-like chain model with a persistence length of 150 bp [62], where the volume fraction $\nu = 0.008$ is comparable to the experimental yeast DNA volume fraction. Fig. S10(b) shows the MSD measured at different values of E_{nonsp} for $\nu = 0.008$. When $E_{\text{nonsp}} \sim 1k_BT$, which corresponds to the non-specific binding energy regime in experiments [63], the effective 3D diffusion coefficient is slightly modified, which does not affect our conclusion on the optimal search process. Additionally, we observed that the MSD curve bends when E_{nonsp} exceeds the typical range of non-specific binding energies.

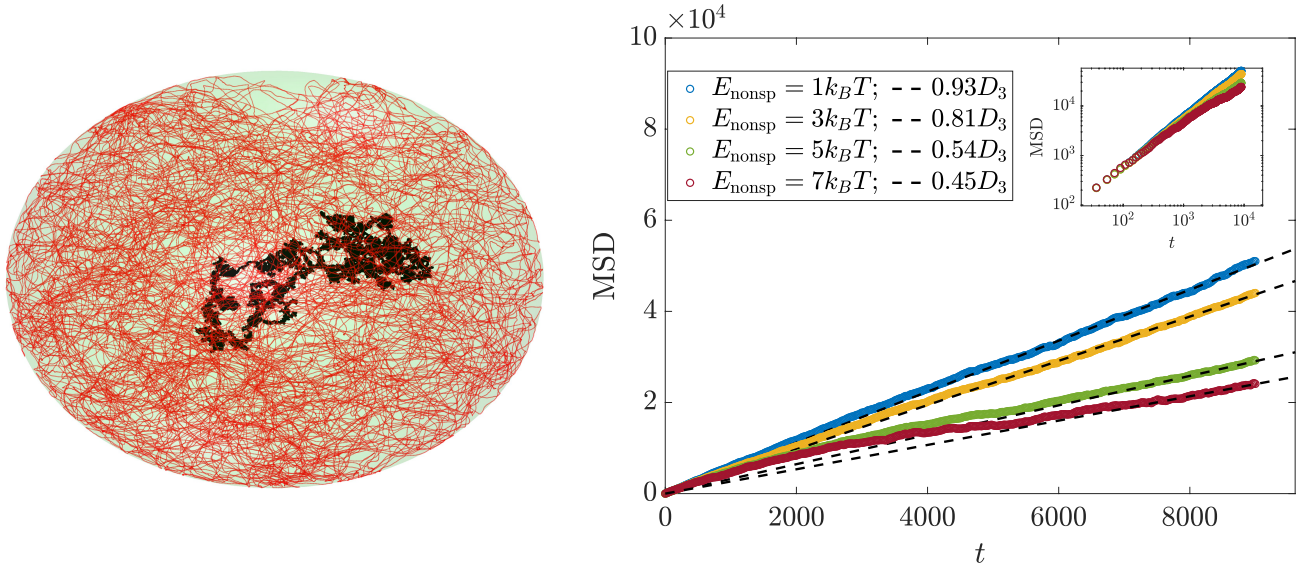

Figure S10: (a) Configuration of DNA (in red) at $\nu = 0.008$ with a complex structure and a trajectory of TF (in black). A TF acts as a point searcher that diffuses in 3D space and becomes trapped once it hits the DNA, which is $1nm$ wide. It detaches at a rate of $\frac{D_3}{1nm^2}\exp(-E_{\text{nonsp}}/k_BT)$. (b) MSD at different E_{nonsp}.

S11. Properties of the octopusing walk

Once an IDR site binds to the antenna, the TF performs an octopusing walk, whereby different IDR binding sites constantly bind and unbind from the DNA. As we shall see, this will lead to an effective 1D diffusion of the TF. This indicates that during the octopusing walk, the TF neither gets trapped on a single target nor fully detaches from the antenna, allowing for rapid dynamics (in fact, the 1D diffusion coefficient can be comparable to the free 3D diffusion coefficient). We shall also show that the number of bound sites on the DNA is described by a probability distribution that is in steady-state and obeys detailed balance.

We denote that time-dependent probability distribution of the number of bound sites by $P(n,t)$ (with n ranging from 0 to $\tilde{n}$). The dynamics of this probability distribution is given by:

$$\frac{dP(n,t)}{dt} = P(n-1,t)W_{n-1,n} + P(n+1,t)W_{n+1,n} + P(n,t)W_{n,n}, \tag{S19}$$

where W is called *transition rate matrix*, and $W_{n,n} = -W_{n,n-1} - W_{n,n+1}$. Intuitively, we anticipate that $W_{n,n-1}$, corresponding to the process of *detachment* of one of the sites, is *linear* in n, since we expect the different sites to be approximately independent of each other. Similarly, if we consider the different IDR sites as independent "searchers", the on-rate (corresponding to $W_{n,n+1}$) to be linear in $(\tilde{n} - n)$. Indeed, Fig. S11(a) corroborates this intuition to an excellent approximation. As the dynamics proceeds, Eq. [S19] would reach a steady-state distribution governed by the matrix W. Fig. S11(b) shows the excellent agreement between the steady-state associated with the matrix W and that found directly from the MD simulation. This confirms that TF movement along the antenna is in a dynamic steady state. We also note that since our transition matrix is tri-diagonal, it satisfies the detailed balance condition, i.e., in the steady-state reached, we have: $P(n)W_{n,n-1} = P(n-1)W_{n-1,n}$, where $P(n)$ is the steady-state distribution.

A *priori*, one may think that the TF is facing two contradictory demands: on the one hand, it has to perform rapid diffusion along the DNA. On the other hand, it needs to bind sufficiently strongly so that it does not fall off the DNA too soon. Indeed, this is known as the speed-stability paradox within the context of TF search in bacteria. Importantly, the simple picture we described above explains an elegant mechanism to bypass this paradox, achieving a high diffusion coefficient with a low rate of detaching from the DNA. This comes about, due to the compensatory nature of the dynamics outlined above: there is, in effect, a feedback mechanism whereby if only few sites are attached to the DNA, the on-rate increases, and, similarly, if too many are attached (thus prohibiting the 1D diffusion) the off-rate increases. This is manifested by the peaked steady-state distribution shown in Fig. S11(b). In fact, this mechanism is remarkably effective even when the typical (i.e., most probable) number of binding sites is as small as 2! (note that in this case, as shown in the inset of Fig. S11(a), the TF may cover a distance of more than 100bp before falling off).

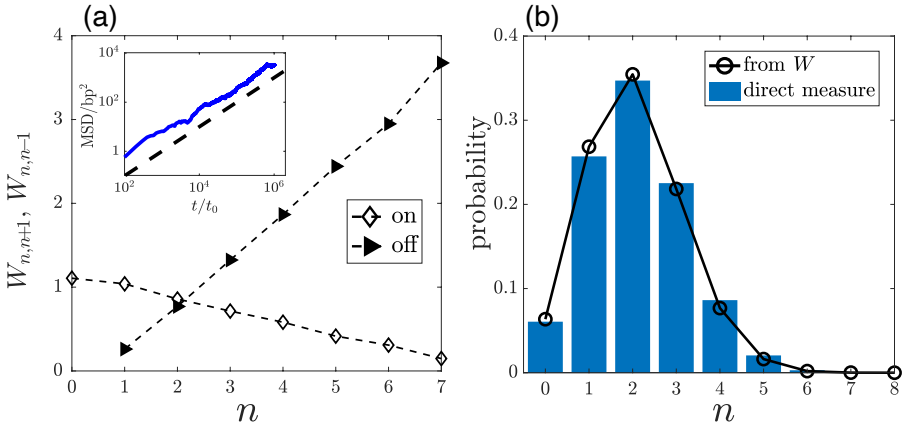

Figure S11: (a) $W_{n,n+1}$ (or $W_{n,n-1}$) denoted by "on" (or "off") varies with n for $E_B = 6$ and $\tilde{n} = 12$. Inset: Mean square displacement (MSD) suggests diffusive motion, as indicated by the dashed line following $\mathrm{MSD} \propto t$. (b) Steady probability distribution of bound sites.

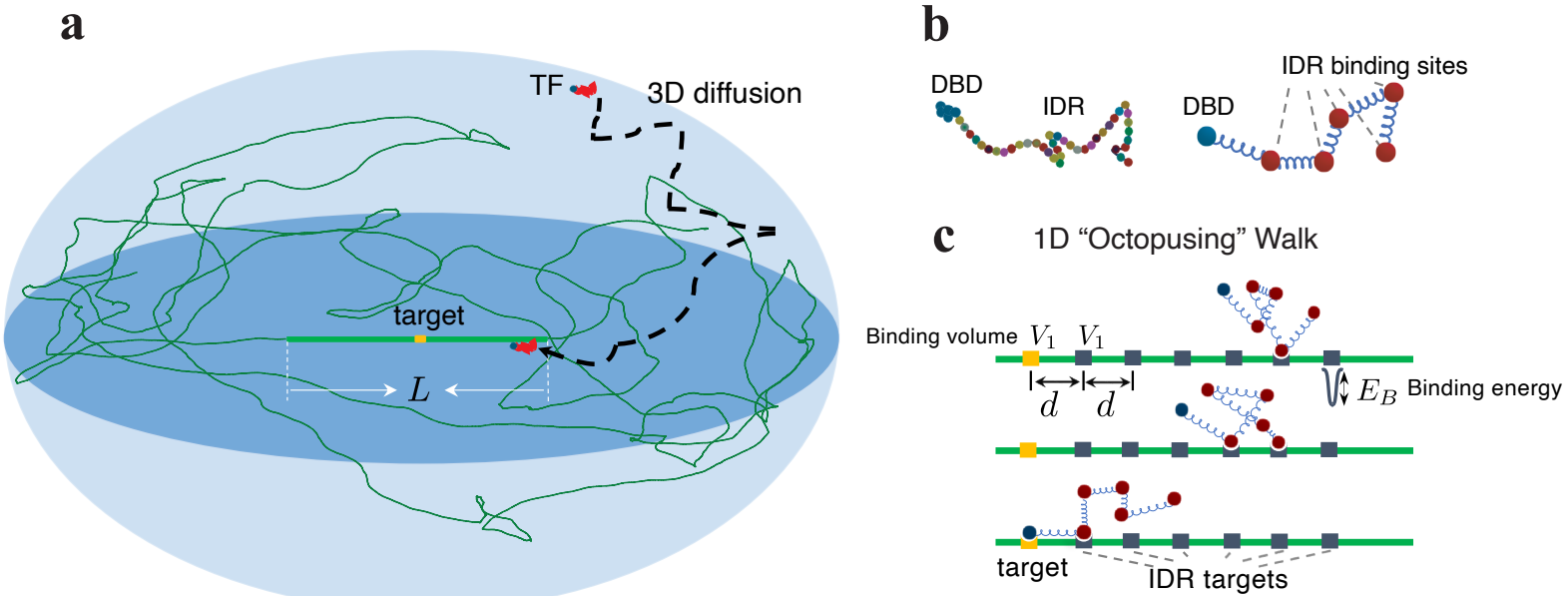
a
TF
3D diffusion
target
L
b
DBD
IDR
DBD
IDR binding sites
c
1D "Octopusing" Walk
Binding volume
V_1
V_1
d
d
E_B
Binding energy
target
IDR targets

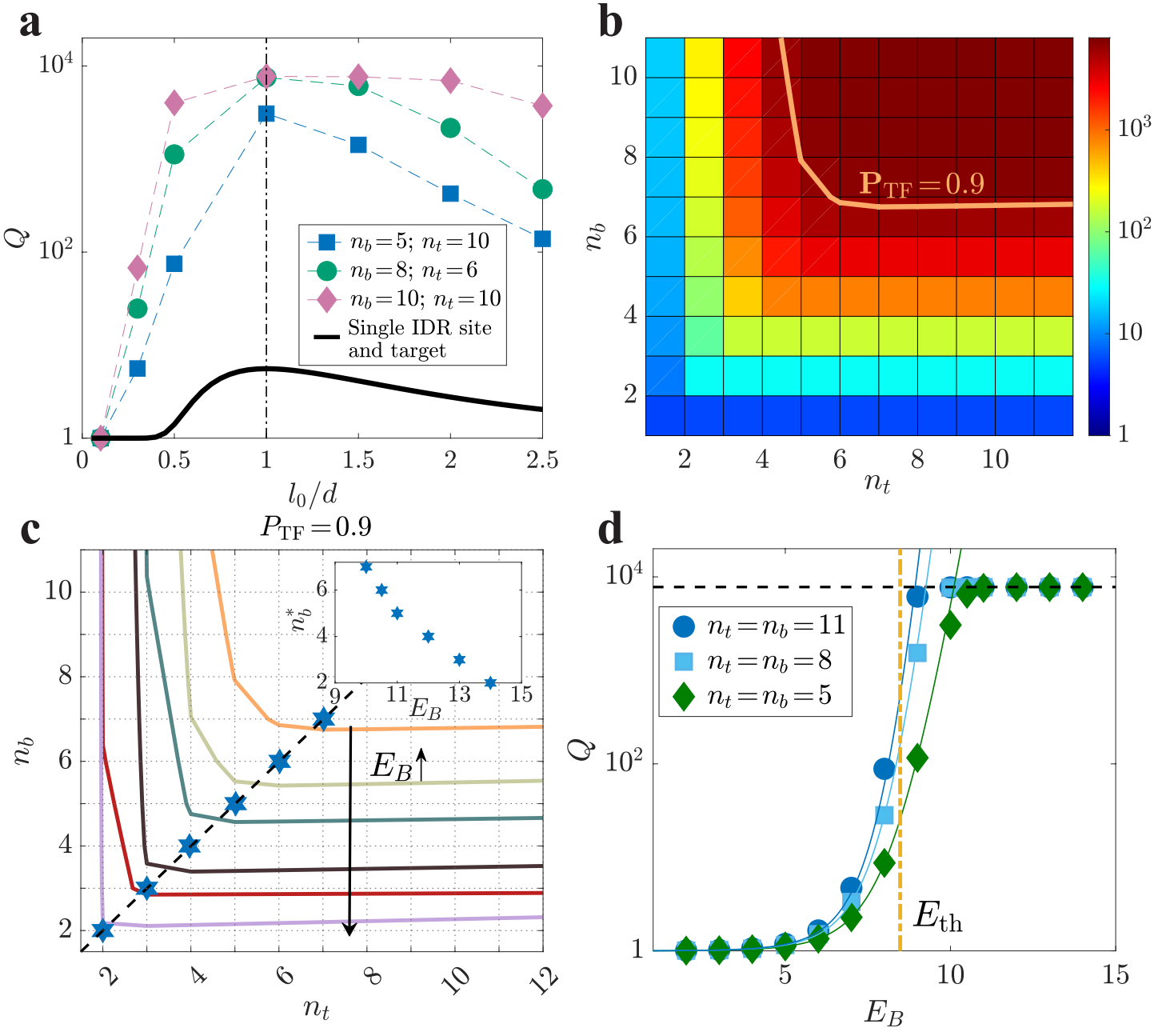
a
10^4
10^2
1
Q
0
0.5
1
1.5
2
2.5
l_0/d
$n_b=5;\ n_t=10$
$n_b=8;\ n_t=6$
$n_b=10;\ n_t=10$
Single IDR site and target
b
n_b
n_t
$P_{\mathrm{TF}}=0.9$
10^3
10^2
10
1
c
$P_{\mathrm{TF}}=0.9$
n_b
n_t
n_b^*
E_B
E_B
d
10^4
10^2
1
Q
5
10
15
E_B
E_{th}
$n_t=n_b=11$
$n_t=n_b=8$
$n_t=n_b=5$

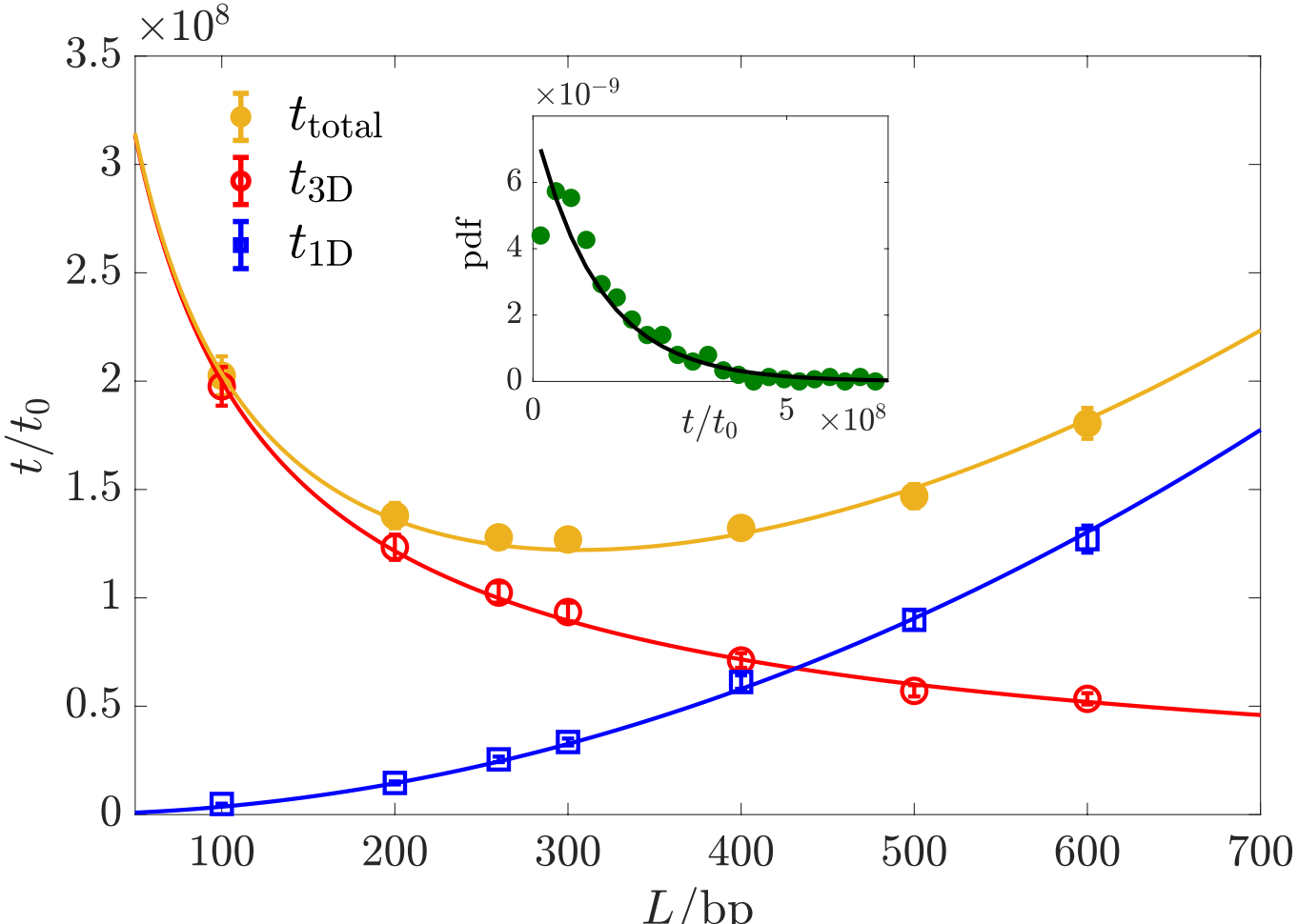
$\times 10^8$
3.5
3
2.5
2
1.5
1
0.5
0
t/t_0
t_{total}
t_{3D}
t_{1D}
$\times 10^{-9}$
6
4
2
0
pdf
0
5
t/t_0
$\times 10^8$
100
200
300
400
500
600
700
L/bp

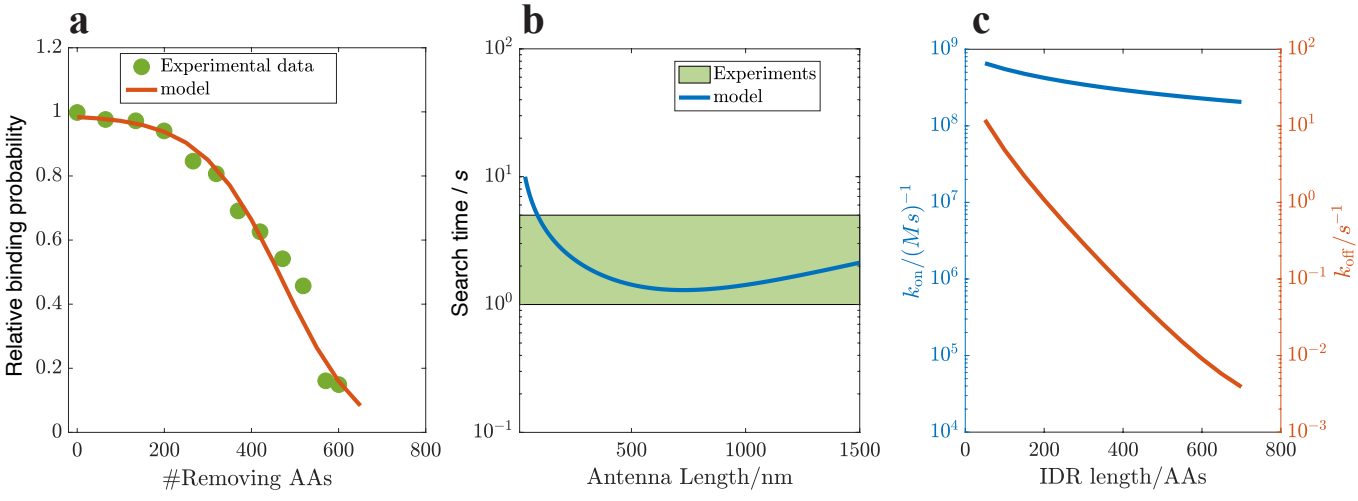
a
Experimental data
model
Relative binding probability
#Removing AAs
b
Experiments
model
Search time / s
Antenna Length/nm
c
$k_{on}/(Ms)^{-1}$
k_{off}/s^{-1}
IDR length/AAs